Link sito dell'editore: https://arc.aiaa.org/doi/10.2514/1.G001018

Link codice DOI: 10.2514/1.G001018

Citazione bibliografica dell'articolo:

Giulio Avanzini, Alessandro Palmas, Elena Vellutini, "Solution of Low-Thrust Lambert Problem with Perturbative Expansions of Equinoctial Elements", Journal of Guidance, Control, and Dynamics, Vol. 38, No. 9, Special Issue in Honor of Richard Battin, Set. 2015, pp. 1585 - 1601

Solution of Low-Thrust Lambert Problem with Perturbative Expansions of Equinoctial Elements

G. Avanzini [1]
Università del Salento, Department of Engineering,

Strada per Monteroni, Complesso Ecotekne - Corpo O, Lecce, Italy

A. Palmas [2] and E. Vellutini [3]
Politecnico di Torino, Department of Mechanical and Aerospace Engineering,

Corso Duca degli Abruzzi 24, 10129, Turin, Italy

A method for solving the so called low-thrust Lambert problem is proposed. After formulating it as a two-points boundary value problem, where initial and final positions are provided in terms of equinoctial variables, a first-order perturbative approach is used for investigating the variation of orbital elements generated by the low-thrust propulsion system, which acts as a perturbing parameter with respect to the zero-order Keplerian motion. An implicit algebraic problem is obtained, which allows for the determination of the low-thrust transfer trajectory that drives the equinoctial parameters from their initial to the final values in a prescribed time. Three test cases are presented, which demonstrate the flexibility of the method for different missions scenarios: an interplanetary transfer from Earth to Mars; a spiral multi-revolution transfer from low Earth orbit to the International Space Station; and a maneuver to a highly elliptical orbit with large plane change.

---

[1] Professor, Università del Salento, Department of Engineering
[2] Graduate Student, Politecnico di Torino, Department of Mechanical and Aerospace Engineering
[3] PhD Student, Politecnico di Torino, Department of Mechanical and Aerospace Engineering

Notation

a	Semi-major axis, km
e	Eccentricity
h	Angular momentum, km^2/s
i	Inclination
ℓ	Mean longitude
L	True longitude
m	Spacecraft mass, kg
p	Parameter or semi-latus rectum, km
P_1, P_2	Equinoctial parameters for eccentricity vector
Q_1, Q_2	Equinoctial parameters for inclination and RAAN
r	Radius, km
R	Reference distance from the primary body, km
t	Time, s
T	Thrust force, N
ToF	Time of flight, s
$\mathbf{u}$	$= (u_r, u_t, u_n)^T$, Acceleration componentes, m/s^2

Greek Symbols

α, β	Thrust azimuth and elevation angles
ΔL	True longitude increment
ε	Acceleration, m/s^2
$\hat{\varepsilon}$	nondimensional acceleration ratio (perturbation parameter)
θ	True anomaly
μ	Mass parameter, km^3/s^2
ω	Argument of periapsis
Ω	Right ascension of the ascending node, RAAN

I. Introduction

This paper provides a novel method for the solution of the two point boundary value problem for low-thrust trajectories. A two-point boundary value problem is solved, as in the case of the classical Lambert problem for ballistic arcs. In the present case boundary conditions are represented by two sets of equinoctial parameters prescribed at initial and final time.

Low-thrust trajectories are attractive in the framework of modern space mission design, since they are associated with efficient and reliable electrical propulsion systems, that represent an interesting choice not only for long interplanetary transfers, such as those required by Smart 1 [1], Hayabusa [2], BepiColombo [3], LISA Pathfinder [4], or transfers to the Moon, but also for missions in proximity of the Earth. Unfortunately mission design becomes more complex in the low-thrust case, where the trajectory depends on the thrust modulus and direction along the whole transfer orbit and it can include multi-revolution trajectories [5].

The classical Lambert problem, as stated by Battin [6], consists in the determination of an orbit having a specified transfer time and connecting two position vectors. This formulation is valid for Keplerian orbits alone, where transfer time is independent of the initial and final orbits and, as demonstrated by Lambert theorem, it depends only on semi-major axis a, the sum of the radii, $r_1 + r_2$, of the initial and final position of the spacecraft, P_1 and P_2, and the length c of the segment joining them. The theorem can be extended to a portion of any conic section and it may include multiple revolutions, performed along the same orbit. Different solution methods were proposed for this classical problem [7–11].

In the low-thrust case the characteristics of the transfer, including transfer time, from the initial to the final position do not depend only on transfer geometry, as in the Keplerian case, but they are a function also of the initial and final orbits and direction and magnitude of the acceleration delivered by the propulsion system. The trajectory can be multi-revolution and the spacecraft can travel around the primary body for a certain number of complete revolutions with orbit parameters constantly varying under the small yet continuous action of the low-thrust electrical engine. The boundary value problem formulated for the low-thrust case has no general closed form solutions and thrust modulus and direction must be treated as unknowns for the problem.

Several authors dealt with the low-thrust orbit transfer problem. In some particular cases, closed form solutions were derived, as for the Stark problem [12]. In other cases, approximate or simplified methods are necessary for achieving analytic or semi-analytic solutions. Among the latter ones, fundamental results were found by Petropoulos and Longuski [13]. Their shape-based method assumes a given trajectory shape that allows for analytically deriving the thrust profile from the equations of motion. Free parameters in the shape function are tuned in order to solve the low-thrust Lambert problem for the given class of transfer trajectories assumed at the beginning. This means that a class of function is assumed *a priori* for trajectory shape and the thrust profile is calculated *a posteriori* in order to follow that particular (class of) path(s).

Following this approach, exact solutions were found by other authors for various classes of shape functions. The most widely used is the exponential sinusoid [14], where radial distance from the central body is expressed as a function of angular travel θ in the orbit plane $r = k_0 \exp[k_1 \sin(k_2\theta + \phi)]$. The function is characterized by three parameters, namely the scale parameter k_0, the dynamic range parameter k_1, and the winding parameter k_2. The phase angle ϕ can be tuned in order to find the most appropriate thrust profile for the particular mission analyzed. This shape function was recently modified by the authors of the present paper [15], in order to derive solutions for low-thrust transfer trajectories in the framework of the circular restricted three-body problem.

The shape-based approach allows for an efficient preliminary analysis of the trajectory design space by means of its analytic solutions and it thus offers a good starting point for trajectory optimization. On the other hand it does not assure the feasibility of the mission. By limiting the value of the product $k_1 k_2^2$, that influences mission geometry, and in particular the curvature of the orbit, it is possible to avoid regions of unfeasible trajectories. Izzo derived an equivalent of Lambert theorem for exponential sinusoids under the assumption of tangential thrust, showing that time of flight is a single-valued monotone function of flight path angle at the initial point γ_1, initial and final radii, r_1 and r_2, and total transfer angle $\bar{\theta} = \psi + 2\pi N$, where N is the number of revolutions around the primary body. The issue of dynamic feasibility for the solution of multi-revolution low-thrust Lambert problems was also highlighted in the framework of a multiple gravity-assist mission optimization [16].

As a further development of the shape-based approach, an algorithm for the solution of low-thrust Lambert problem by means of exponential sinusoids was proposed by Vasile et al. [17]. Given the initial and final distance from the primary body, r_1 and r_2, the number of revolutions N and time of flight, thrust profile, total Δv and initial and final velocity vectors v_1 and v_2 were computed. Again, mission feasibility needs to be assessed, taking into account that the exponential sinusoid shape may result into solutions with a large number of revolutions around the primary body. This can be avoided by providing adequate bounds to the parameter k_2, with the further advantage of reducing the size of the search space. As a further contribution, Ref. [17] also introduces a shape method based on a prescribed variation of pseudo-equinoctial parameters, that do not satisfy exactly Gauss's planetary equations. A formulation of the low-thrust Lambert problem was derived also for the pseudo-equinocital parameters in terms of a minimum-fuel prescribed time orbit transfer. As a result, the analytical solutions derived through shape-based methods (including those based on pseudo-equinoctial parameter shaping) are valid only for the specific class of shape functions considered and they cannot cover all possible spacecraft trajectories.

A perturbative expansion is proposed in the present paper for deriving an analytical description of the evolution of orbital equinoctial parameters under the action of a low-thrust propulsion system. This approach allows for a good approximation of the trajectory shape without the need for any *a priori* assumption on the trajectory geometry. This is a major difference with respect to shape-based methods, where trajectory arcs are prescribed by means of a given (class of) shape function(s), such as the exponential sinusoid proposed in [13]. Low-thrust acceleration $\varepsilon = T/m$ is chosen as the perturbation parameter. Zero order (constant) terms in the perturbative expansions developed for each orbit parameter represent the reference Keplerian motion, with constant orbit parameters for $\varepsilon = 0$. The first order terms take into account the perturbing effect of low-thrust on the evolution of orbit parameters. This approach allows one investigating the solution of the low-thrust Lambert problem for a prescribed transfer time and a given set of boundary conditions expressed in terms of equinoctial parameters, which univocally identify the initial and final positions along given orbits.

Zuiani et al. preliminarily tested the consistency of the perturbative expansion for multi-objective optimization of low-thrust trajectories [18], for a mission not requiring a significant plane

change. An extension of the approach for including the effects of constant thrust in either an inertially fixed or a rotating frame, while taking into account J2 perturbations on the resulting spacecraft motion, is discussed in [19]. The objective of the present work is, first of all, to describe in more detail the perturbative expansions, discussing for the first time the derivation of all the terms, while highlighting the potential of the method to solve numerically demanding problems with good accuracy and a relatively limited amount of computational effort. An improved version of the estimate of transfer time will also be introduced, with respect to Ref. [18]. At the same time the method here proposed represents to the best of the authors' knowledge the first technique developed in the literature for rephrasing the low-thrust Lambert problem in terms of a two-point boundary-value problem, thus closely resembling the Keplerian case, rather than stating it in the form of a (possibly multi-objective) constrained optimization problem with prescribed transfer time.

Spacecraft path is divided into a number of elements and the trajectory is calculated by means of centered perturbative expansions. Many tools for low-thrust mission preliminary design are based on some form of trajectory discretization, but in many cases the trajectory is divided into a sequence of ballistic Keplerian arcs, and the action of the low-thrust propulsion system is represented by means of finite velocity increments at the bounds of each interval [20]. On the converse, continuity conditions for the whole set of orbit parameters at break points of transfer arcs allows the algorithm here presented to determine a smooth trajectory, where the effects of low-thrust are analytically evaluated over the whole trajectory. An analytical approximation of the evolution of classical orbital elements under the action of low-thrust was derived also by Yang Gao [21] by means of a technique based on averaging, which suits multi-revolution planar orbit transfers with tangential acceleration. In this respect, the perturbative expansions derived in this work allows for taking into account arbitrary acceleration components in the radial, transverse, and normal-to-the-orbit-plane directions.

An implicit problem is thus derived from the discretization of the whole trajectory into low-thrust arcs, where total transfer time is enforced as a constraint. The resulting set of algebraic conditions can be solved by any numerical iteration scheme, such as Newton-Raphson method or Sequential Quadratic Programming (SQP) algorithm [22]. The thrust profile is evaluated without

imposing limitations, since thrust now becomes one of the unknowns for the problem, which influences the evolution of the whole orbit. As a further advantage, large thrust variations are expected, when using shape-based solutions, whereas a constant acceleration profile can be imposed in the present case over most of the trajectory, a situation that resembles more closely the actual thrust profile of a space mission featuring an propulsion system that delivers a prescribed thrust force that usually cannot be modulated.

The technique proposed in this paper shares some similarities with the collocation method adopted in many papers for solving an optimal control problem by means of nonlinear programming (NLP) algorithms (among many others, we only cite here the works by Enright and Conway [23] and Tang and Conway [24], referring the reader to these works and references therein for further details on collocation methods). When direct collocation is used, a set of polynomial functions (e.g. Hermite cubic polynomials) is adopted for discretizing the trajectory over several intervals, with linearly varying control action over the interval, [23] thus providing continuity on trajectory variables and their derivatives at endpoints (nodes), while enforcing the equations of motion at mid-points of the intervals (collocation points) during the solution of the NLP problem. This is similar to what is done in the present method, in terms of discretizing the trajectory by means of a set of arcs, with the derivation of a finite order set of algebraic equations. As a difference, the perturbative approach allows for deriving a variation of orbit parameters over a given true longitude increment which is based on physical properties of the system over the whole arc, rather than exactly enforcing the equations of motion at some discrete points only. In both case, the accuracy of the solution becomes higher, when shorter intervals are used.

Together with numerical performance and accuracy, the paper also analyzes possible limitations of the method and ways for circumventing them. In particular, the perturbation parameter ε is assumed constant along each arc and the error in the approximation increases with ε. Hence, for a given accuracy, the angular amplitude of the arc is not a free parameter, but it should be varied, depending on thrust modulus. An analysis of the effect of the variation of discretization arc amplitude with distance from the primary body is thus carried out in the final part of the paper. Also note that perturbative expansions of equinoctial parameters allow managin thrust as either a

prescribed parameter or as a design variable, without the need for varying it in order to follow a prescribed trajectory arc. The shape of the arc is determined in the present case by an approximate perturbative expansion based on Gauss equations for the evolution of equinoctial elements, and as such is dictated solely by the physical properties of the system. The price to pay with respect to the shape-based method is the need for a numerical solution scheme of the implicit algebraic problem derived from the discretization of the trajectory, that replaces the analytical solution available for the exponential sinusoid or other shape functions considered in the literature.

In the sequel the perturbative expansions of equinoctial elements will be derived and Lambert problem for low-thrust trajectories will be stated. Then the low-thrust transfer problem discretization will be defined in Section III, discussing numerical issues of the method employed for solving the problem. Finally the results obtained for a few test-cases are critically analyzed. Some concluding remarks end the paper.

II. Perturbative Expansions of Equinoctial Elements

A. Fundamental equations and geometry of the problem

Assuming the semi-major axis a as the first equinoctial parameter, the remaining 5 parameters are expressed in terms of classical orbital elements as [6]

$$\begin{aligned} P_1 &= e\,\sin(\Omega+\omega) \\ P_2 &= e\,\cos(\Omega+\omega) \\ Q_1 &= \tan(i/2)\,\sin\Omega \\ Q_2 &= \tan(i/2)\,\cos\Omega \\ L &= \Omega+\omega+\theta \end{aligned} \tag{1}$$

Their evolution depends on acceleration components $\mathbf{u} = (u_r, u_t, u_n)^T$ in the radial, transverse, and normal directions, respectively (where the normal direction n is perpendicular to the orbit plane, that is, parallel to the orbit angular momentum $\mathbf{h}$), through a set of variational equations [25],

$$\frac{da}{dt} = \frac{2a^2}{h}\left[(P_2\sin L - P_1\cos L)\,u_r + \frac{p}{r}u_t\right]$$

$$
\begin{aligned}
\frac{dP_1}{dt} =& \frac{r}{h}\left\{-\frac{p}{r}\cos L\, u_r + \left[P_1 + \left(1+\frac{p}{r}\right)\sin L\right] u_t - P_2\left(Q_1\cos L - Q_2 \sin L\right) u_n\right\} \\
\frac{dP_2}{dt} =& \frac{r}{h}\left\{\frac{p}{r}\sin L u_r + \left[P_2 + \left(1+\frac{p}{r}\right)\cos L\right] u_t + P_1\left(Q_1\cos L - Q_2 \sin L\right) u_n\right\} \\
\frac{dQ_1}{dt} =& \frac{r}{2h}\left(1+Q_1^2+Q_2^2\right)\sin L\, u_n \\
\frac{dQ_2}{dt} =& \frac{r}{2h}\left(1+Q_1^2+Q_2^2\right)\cos L\, u_n \\
\frac{d\ell}{dt} =& \sqrt{\frac{\mu}{a^3}} - \frac{r}{h}\left(Q_1\cos L - Q_2\sin L\right) u_n
\end{aligned}
\tag{2}
$$

Letting $\varepsilon = T/m$ be the magnitude of the acceleration, where T and m are thrust and spacecraft mass, respectively, the components of $\mathbf{u}$ in the radial-transverse-normal frame are given by

$$
\mathbf{u} = (u_r, u_t, u_n)^T = \varepsilon\left(\cos\alpha\,\cos\beta, \sin\alpha\,\cos\beta, \sin\beta\right)^T \tag{3}
$$

where α and β are azimuth and elevation of the acceleration, respectively (Fig. 1). In order to derive a perturbation expansion where all the terms have consistent dimensions (i.e. in $x = x_0 + \hat{\varepsilon}x_1 + \mathcal{O}(\hat{\varepsilon}^2)$, the variables x, x_0, and x_1 are expressed in the same units), a non-dimensional acceleration ratio

$$
\hat{\varepsilon} = (T/m)/(\mu/R^2), \tag{4}
$$

is introduced, equal to the ratio between thrust acceleration and gravity pull at a reference distance R from the primary body. Variation of orbital elements is then expanded up to first order in $\hat{\varepsilon}$.

B. First-order perturbation terms

The set of ordinary differential equations (ODEs) in Eq. (2) can be numerically integrated to determine the evolution of equinoctial variables. However it would be highly desirable to have a computationally more efficient way to describe orbital motion for missions that require long thrusting phases, as in the low-thrust case. The perturbative approach provides an approximate solution for the equations of motion in a shorter computational time, at the cost of a reduced accuracy in comparison with a direct numerical integration method.

First of all, a change in the independent variable of the problem is performed by means of the

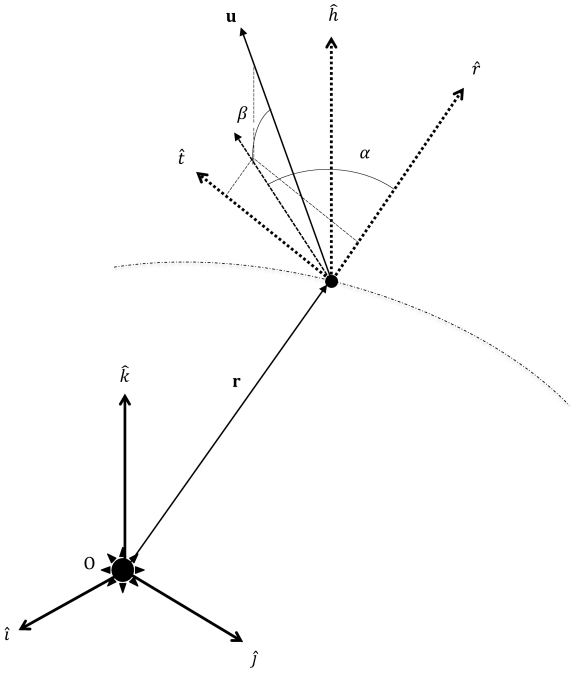

Fig. 1 Radial transversal reference frame.

derivative chain rule, where

$$\frac{d}{dt}(x) = \frac{d}{dL}(x)\,\frac{dL}{dt} \;\Rightarrow\; \frac{d}{dL}(x) = \frac{1}{\dot{L}}\,\frac{d}{dt}(x) \tag{5}$$

with $\dot{L} \approx h/r^2$ and x equal to either a, P_1, P_2, Q_1, or Q_2. Note that a complete expression of $\dot{L} = (\dot{L})_0 + \hat{\varepsilon}(\dot{L})_1$ should also feature first order in $\hat{\varepsilon}$ terms, related to the perturbing acceleration. But when this expression is substituted into Eq. 5, all the $\hat{\varepsilon}$ terms of $1/\dot{L} = 1/(\dot{L})_0 - \hat{\varepsilon}/(\dot{L})_1 + \mathcal{O}(\hat{\varepsilon}^2)$ are multiplied times $d(x)/dt$, which in turn is proportional to $\hat{\varepsilon}$, thus generating second order terms in $\hat{\varepsilon}$, which are dropped. Consequently, only the zero-order term is retained in the expression of $\dot{L}$ for a consistent expansion, first-order accurate in $\hat{\varepsilon}$.

All the variational equations for equinoctial orbit parameters are thus expressed in terms of derivatives with respect to the true longitude, L, rather than time, t. The first 5 equinoctial parameters are then expanded up to first order perturbations with respect to $\hat{\varepsilon}$, in the form

$$a = a_0 + \hat{\varepsilon} a_1$$

$$P_1 = P_{10} + \hat{\varepsilon} P_{11}$$

$$
\begin{aligned}
P_2 &= P_{20} + \hat{\varepsilon} P_{21} \\
Q_1 &= Q_{10} + \hat{\varepsilon} Q_{11} \\
Q_2 &= Q_{20} + \hat{\varepsilon} Q_{21}
\end{aligned} \tag{6}
$$

where the constant terms with subscript 0 provide the values of the equinoctial parameters for L_0, whereas the values of the first order terms, with subscript 1 provide an estimate of the effect of low-thrust on the evolution of orbit parameters. When $\hat{\varepsilon} = 0$, all the orbit parameters describing shape and position of the orbit remain constant and the Keplerian solution is recovered. The first order terms in the expansions are computed by applying standard perturbation theory [26, 27] to the set of differential equations given by Eq. (2), where all the expansions in the form $x(L, L_0; \hat{\varepsilon}) = x_0 + \hat{\varepsilon} x_1(L, L_0)$ introduced in Eqs. (6)are substituted in Eqs. (2) and only first order terms in $\hat{\varepsilon}$ are retained. When parameter x appears in a nonlinear term, a Taylor series expansion in $\hat{\varepsilon}$ is adopted. As an example, in the first of Eqs.(2) one writes $a^2 = a_0 + \hat{\varepsilon} a_1 + \mathcal{O}(\hat{\varepsilon}^2)$.

When $R = a_0$ is assumed in the expression of the nondimensional acceleration ratio $\hat{\varepsilon}$, and after higher order terms in $\hat{\varepsilon}$ are dropped, the evolution of equinoctial parameters for constant values of $\hat{\varepsilon}$, α, and β is expressed as:

$$
\begin{aligned}
a(L, L_0; \hat{\varepsilon}) =& a_0 + \hat{\varepsilon} \cdot 2a_0(1 - P_{10}^2 - P_{20}^2) \cos\beta \left[\cos\alpha \left(P_{20} I_{s2} - P_{10} I_{c2}\right) + \sin\alpha I_{11}\right] \\
P_1(L, L_0; \hat{\varepsilon}) =& P_{10} + \hat{\varepsilon} \cdot (1 - P_{10}^2 - P_{20}^2)^2 \cdot \\
& \cdot \{\cos\beta \left[\sin\alpha \left(P_{10} I_{13} + I_{s2} + I_{s3}\right) - \cos\alpha I_{c2}\right] + \sin\beta P_{20} \left(Q_{20} I_{s3} - Q_{10} I_{c3}\right)\} \\
P_2(L, L_0; \hat{\varepsilon}) =& P_{20} + \hat{\varepsilon} \cdot (1 - P_{10}^2 - P_{20}^2)^2 \cdot \\
& \cdot \{\cos\beta \left[\cos\alpha I_{s2} + \sin\alpha \left(P_{20} I_{13} + I_{c2} + I_{c3}\right)\right] + \sin\beta P_{10} \left(Q_{10} I_{c3} - Q_{20} I_{s3}\right)\} \\
Q_1(L, L_0; \hat{\varepsilon}) =& Q_{10} + \hat{\varepsilon} \cdot 2(1 - P_{10}^2 - P_{20}^2)^2 \sin\beta I_{s3} \left(1 + Q_1^2 + Q_2^2\right) \\
Q_2(L, L_0; \hat{\varepsilon}) =& Q_{20} + \hat{\varepsilon} \cdot 2(1 - P_{10}^2 - P_{20}^2)^2 \sin\beta I_{c3} \left(1 + Q_1^2 + Q_2^2\right)
\end{aligned} \tag{7}
$$

The quantities $I_{11}, I_{12}, I_{13}, I_{s2}, I_{s3}, I_{s5}, I_{c2}, I_{c3}$ and I_{c5} can be obtained analytically from finite integrals evaluated between initial and current values of true longitude L for the considered arc:

$$
I_{11}\left(L, L_0\right) = \int_{L_0}^{L} \frac{1}{\left(1 + P_{10} \sin L + P_{20} \cos L\right)} \, dL,
$$

$$
\begin{aligned}
I_{12}\left(L, L_0\right) &= \int_{L_0}^{L} \frac{1}{\left(1 + P_{10}\sin L + P_{20}\cos L\right)^2}\, dL, \\
I_{13}\left(L, L_0\right) &= \int_{L_0}^{L} \frac{1}{\left(1 + P_{10}\sin L + P_{20}\cos L\right)^3}\, dL, \\
I_{s2}\left(L, L_0\right) &= \int_{L_0}^{L} \frac{\sin L}{\left(1 + P_{10}\sin L + P_{20}\cos L\right)^2}\, dL, \\
I_{s3}\left(L, L_0\right) &= \int_{L_0}^{L} \frac{\sin L}{\left(1 + P_{10}\sin L + P_{20}\cos L\right)^3}\, dL, \\
I_{s5}\left(L, L_0\right) &= \int_{L_0}^{L} \frac{\sin L}{\left(1 + P_{10}\sin L + P_{20}\cos L\right)^5}\, dL, \\
I_{c2}\left(L, L_0\right) &= \int_{L_0}^{L} \frac{\cos L}{\left(1 + P_{10}\sin L + P_{20}\cos L\right)^2}\, dL, \\
I_{c3}\left(L, L_0\right) &= \int_{L_0}^{L} \frac{\cos L}{\left(1 + P_{10}\sin L + P_{20}\cos L\right)^3}\, dL, \\
I_{c5}\left(L, L_0\right) &= \int_{L_0}^{L} \frac{\cos L}{\left(1 + P_{10}\sin L + P_{20}\cos L\right)^5}\, dL.
\end{aligned}
\tag{8}
$$

Closed-form expressions for these integrals are can be obtained with the help of a mathematical manipulation software. As an example, the primitive of the argument of the first integral in Eq. (14), namely $\varphi_{11}(L) = \left(1 + P_{10}\sin L + P_{20}\cos L\right)^{-1}$, is given by

$$
\Phi_{11}(L) = \begin{cases}
-\dfrac{2}{\sqrt{\sigma}} \arctan\left(\dfrac{(P_{20}-1)\sin L - P_{10}\cos L - P_{10}}{\sqrt{\sigma}(\cos L + 1)}\right) & \text{if} \quad \sigma > 0 \\
\dfrac{1}{\sqrt{-\sigma}} \log\left[\dfrac{(\sqrt{-\sigma} - P_{10})\cos L + (P_{20}-1)\sin L + \sqrt{-\sigma} - P_{10}}{(\sqrt{-\sigma} + P_{10})\cos L + (1 - P_{20})\sin L + \sqrt{-\sigma} + P_{10}}\right] & \text{if} \quad \sigma \leq 0
\end{cases}
$$

with $\sigma = 1 - P_{10}^2 - P_{20}^2$. Note that for $\sigma \to 0$ the solution is singular for the first expression, but a finite limit is available in the second case. The expression for $I_{11}(L, L_0)$ is thus always available in closed form, and it is given by

$$
I_{11}(L, L_0) = \Phi_{11}(L) - \Phi_{11}(L_0).
$$

When P_{10} and P_{20} are expressed in terms of classic orbit parameters, it is $\sigma = 1 - e^2$. Only cases with eccentricity less than 1 will be considered in the next section. This means that only the first expression of the primitive will be used in the sequel. The expressions of the remaining integrals, omitted here for the sake of conciseness, follow a similar (or simpler) pattern. These expressions, reported in Ref. [28], will be employed for the study of the evolution of the equinoctial parameters for the low-thrust Lambert problem.

C. Evolution of time

The equation for time is now expressed in the form

$$\frac{dt}{dL} = \frac{1}{\dot{L}} = \frac{h^3}{\mu^2(1 + P_1 \sin L + P_2 \cos L)^2} \tag{9}$$

The transfer time along the low-thrust trajectory arc can thus also be expressed as

$$t = t_0 + \hat{\varepsilon} t_1 \tag{10}$$

where t_0 is the transfer time from L_0 to L on the Keplerian orbit with parameters a_0, P_{10}, P_{20}, Q_{10}, and Q_{20}. By expanding all the terms up to first order in $\hat{\varepsilon}$ one gets

$$t(L, L_0; \hat{\varepsilon}) = t_0 - \hat{\varepsilon} \left\{ \left[h_0^7/(a_0^2 \mu^4) \right] (Q_{20} I_{s5} - Q_{10} I_{c5}) \sin\beta / I_{12} + t_{12} \right\} \tag{11}$$

where the last term t_{12} in first-order perturbative expansion of time [see the last equation in Eq. (7)] can be expressed in the form

$$t_{12} = - \left[h_0^3/(2\mu^2) \right] (K_1 + K_2 + K_3 + K_4 + K_5 + K_6)$$

where the six coefficients K_i, $i = 1, \ldots, 6$ depend on finite integrals apparently similar to those defined for the other equinoctial parameters. As an example, the expression of K_1 is

$$K_1 = (1 - P_{10}^2 - P_{20}^2) \left(C_{c_{c3}} I_{c_3 i F_c} + C_{c_{s3}} I_{s_3 i F_c} + C_{c_{c2}} I_{c_2 i F_c} + C_{c_{s2}} I_{s_2 i F_c} + C_{c_{11}} I_{1_1 i F_c} + C_{c_{13}} I_{1_3 i F_c} \right)$$

where the coefficients $C_{(\cdot)}$ are given by

$$\begin{aligned}
C_{c_{11}} =& 12 P_{20} \sin\alpha \cos\beta \\
C_{c_{13}} =& -4 P_{20} (1 + 2P_{20}^2 + 2P_{10}^2) \sin\alpha \cos\beta \\
C_{c_{c2}} =& 4 \left[P_{20} (P_{10}^2 - 1 - 2P_{20}^2) \sin\alpha - 6 P_{10} P_{20} \cos\alpha \right] \cos\beta \\
C_{c_{s2}} =& -4 \left[(1 - P_{10}^2 - P_{20}^2) \cos\alpha + 3 P_{10} P_{20 \sin\alpha} \right] \cos\beta \\
C_{c_{c3}} =& -4 \left[P_{10} Q_{10} (1 - P_{10}^2 - P_{20}^2) \sin\beta + (1 - P_{10}^2 + 2P_{20}^2) \sin\alpha \cos\beta \right] \\
C_{c_{s3}} =& 4 \left[P_{10} Q_{20} (1 - P_{10}^2 - P_{20}^2) \sin\beta - 3 P_{10} P_{20} \sin\alpha \cos\beta \right]
\end{aligned}$$

whereas the quantities $I_{c_3 i F_c}, I_{s_3 i F_c}, I_{c_2 i F_c}, I_{s_2 i F_c}, I_{1_1 i F_c}, I_{1_3 i F_c}$ represent finite integrals of trigonometric and transcendental functions of true longitude, L. The expression of the integral $I_{c_3 i F_c}$ is

reported as example, where

$$
\begin{aligned}
I_{c_3 i F_c}(L, L_0) \;=\; & \int_{L_0}^{L} \{-3P_{20}\log[(\sqrt{\sigma}-P_{10})\cos L+(P_{20}-1)\sin L+\sqrt{\sigma}-P_{10}]/(2\sigma^{5/2})+ \\
+\; & 3P_{20}\log[(\sqrt{\sigma}+P_{10})\cos L+(1-P_{20})\sin L+\sqrt{\sigma}+P_{10}]/(2\sigma^{5/2})+ \\
+\; & [P_{10}(P_{10}^4+P_{10}^2P_{20}(2P_{20}^2+P_{20}-2)+P_{20}(P_{20}^4+4P_{20}^3-5P_{20}^2-P_{20}+1))\cos L^2+ \\
+\; & P_{20}^2\cos L((2P_{10}^4+2P_{10}^2(2P_{20}^2+P_{20}-3)+2P_{20}^4-4P_{20}^3+3P_{20}^2-2P_{20}+1)\sin L+ \\
+\; & P_{10}(2P_{10}^2+5P_{20}^2-5))+P_{10}(P_{10}^4(P_{20}+1)+4P_{10}^2P_{20}(P_{20}^2-1)+ \\
+\; & P_{20}(2P_{20}^4-3P_{20}^3+2P_{20}^2-3P_{20}+2))\sin L^2+P_{20}(2P_{10}^4+2P_{10}^2(3P_{20}^2-P_{20}-2)+ \\
+\; & P_{20}^4-2P_{20}^3+3P_{20}^2-4P_{20}+2)\sin L-P_{10}(P_{10}^4+P_{10}^2P_{20}(2P_{20}^2-P_{20}-2)+ \\
+\; & P_{20}(P_{20}^4-P_{20}^3-5P_{20}^2+P_{20}+1))]/4(2P_{20}(P_{10}^2+P_{20}^2-1)^2(P_{20}-1)^2(P_{20}\cos L+ \\
+\; & P_{10}\sin L+1)^2)\}\cos L/(1+P_{10}\sin L+P_{20}\cos L)^4\,dL
\end{aligned}
$$

A closed form solution for these kind of integrals cannot be found. This means that they need to be evaluated by means of numerical quadrature. From the computational point of view, this becomes by far the most expensive part of the calculations in terms of floating point operations (FLOPS), representing the largest portion of the CPU time necessary for propagating orbit parameters under low thrust with the perturbative approach.

The computational burden is increased by the tight accuracy necessary for a correct evaluation of the integrals. Figure 2 represents the relative error in the evaluation of time along a trajectory arc L. The test is carried out starting from a circular low Earth orbit with $R = 7500$ km and a perturbation parameter $\hat{\varepsilon} = 10^{-5}$. The error is defined as $\Delta\hat{t} = |t_P - t_F|/t_F$, where the exact value t_F is obtained from a high-order accurate numerical propagation by means of Encke's method, whereas t_P is the approximate value derived from the expansion of time in Eq. (11). Three expressions for t_P has been considered in this analysis, namely $t_P = t_0$, where only the zero-th order term is retained; $t_P = t_0 - \varepsilon t_{11}$, where $t_{11} = \left[h_0^7/(a_0^2\mu^4)\right](Q_{20}I_{s5} - Q_{10}I_{c5})\sin\beta/I_{12}$ is the first term in the perturbative expansion of time, and, finally, $t_P = t_0 - \varepsilon(t_{11} + t_{12})$, where the integrals in t_{12} are evaluated numerically by means of quadrature.

The error for the zero-order estimate of time clearly grows faster than that featuring a first-order

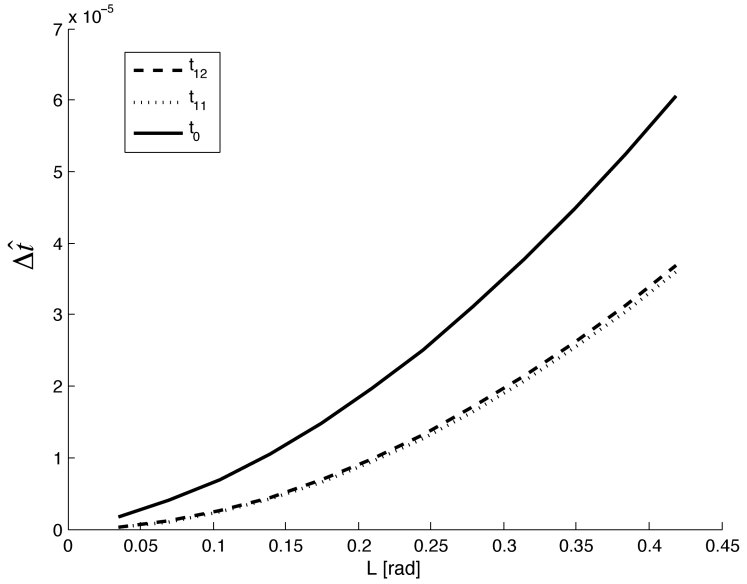

Fig. 2 Comparison of error in time of perturbed expansion.

correction, proportional to the intensity of the perturbation term. When a fast quadrature scheme is adopted, with a coarse relative tolerance equal to 10^{-3}, the term t_{12} decreases the accuracy, rather than improving it, with respect to the estimate based on the use of the term t_{11} alone. This is clearly visible in Fig. 2, where the dotted line labelled t_{11} remains constantly below the dashed one, representing the (ideally more accurate) solution that features one additional correcting term.

It is necessary to significantly tighten the tolerance on the evaluation of the integrals up to 10^{-10} in order to get better results, but the improvement in term of accuracy is marginal, at the cost of an increased computational burden. The curve for the refined values of t_{12} almost perfectly overlaps that featuring t_{11} alone and it is thus omitted. Provided that the improvement obtained from the term t_{12} is very modest (if any) and conversely computational time required by its evaluation is significant, only the first term t_{11}, available in closed form, is used in the perturbative expansion of time, which provides a significant improvement over the zero-order term used in [18], at negligible computational cost.

D. Accuracy of the expansion

The first order expansions of five equinoctial parameters can be propagated backward and/or forward as a function of true longitude, L, in order to obtain the position of the spacecraft and,

thanks to the time equation developed above, the corresponding transfer time over the same low-thrust trajectory arc. The error on the evaluation of time was analyzed above. Provided that the whole arc is described starting from orbit parameters evaluated at the initial point used for the propagation, also the error on the estimate of the position of the spacecraft grows with angular travel from the initial position, for a given set of starting orbit parameters and low-thrust acceleration.

The accuracy of the expansion thus needs to be addressed in order to keep the error under control. This issue has been investigated in some detail by Zuiani *et al.* [18] and the analysis is thus not reported here, for the sake of conciseness. Reference [18] shows that the error increases superlinearly with $\hat{\varepsilon}$ and size of the increment ΔL used for the expansion. Accuracy remains good even for long transfer arcs, when $\hat{\varepsilon}$ lies in a range below 10^{-4}. When higher values of ε are dealt with, only a coarse approximation of the actual trajectory becomes available over multiple revolutions, which nonetheless still suits preliminary studies. As an alternative, when long transfer arcs need to be dealt with, some form of discretization of the trajectory can be used, in order to keep the overall error along the trajectory within acceptable limits. This possibility is investigated in the next section, after the novel formulation for the low-thrust Lambert problem is introduced.

III. Solution Scheme for the Low-Thrust Lambert Problem

A. Problem Discretization

As discussed above, the accuracy of the perturbative expansion decreases with perturbation parameter size and true longitude increments. Hence, the expansions presented in Eq. (7) cannot usually be applied to the whole transfer arc, even if the values of thrust parameters, ε, α and β remain constant along the trajectory. It is thus necessary to divide the spacecraft path into a certain number of arcs in order to propagate the equinoctial elements along each one of them with a reasonable bound on the resulting error. For each arc element, magnitude, azimuth and elevation of thrust over the orbit plane are assumed as constant. The number of arcs used for orbit discretization depends on the required accuracy and total expected angular travel. A higher number of trajectory arcs produces more accurate results, but it also increases the order of the algebraic system that needs to be solved, making its solution computationally more demanding. Uniform increments for

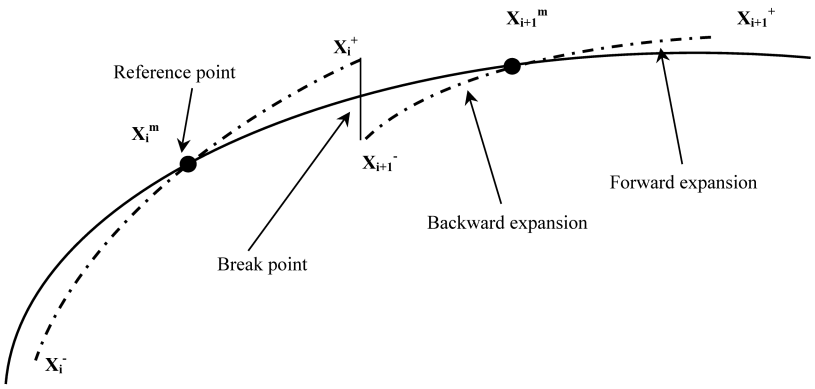

Fig. 3 Centered expansion and matching conditions at the bounds.

true longitude, ΔL, will be initially considered.

The expansion is centered at the mid-point of each discretization arc. The choice of a centered expansion, instead of forward expansion only is motivated by (i) better numerical stability with respect to the shooting problem defined when forward expansions only are used and (ii) better numerical accuracy for the perturbative expansion. In this latter respect, and remembering that the error increases superlinearly with ΔL, the overall propagation error over a given trajectory arc ΔL is smaller when backward and forward propagations of size $\Delta L/2$ are used instead of a single one-directional propagation that covers the whole trajectory arc, ΔL.

For each arc element of angular amplitude ΔL, the mid-point is thus chosen as the starting point for backward and forward propagation along half of the angular travel, $\Delta L/2$. The endpoints of each arc are the points of conjunction between the forward expansion of element k for the discretized trajectory with the backward expansion of the following element, $k+1$, as shown in Fig. 3. The expansions of the equinoctial parameters thus achieve the structure represented in compact form by the equation

$$\begin{cases} \mathbf{X}^{+} = \mathbf{X}^{m} + \varepsilon\, \mathbf{f}\left(\mathbf{X}^{m}, \Delta L/2, \varepsilon, \alpha, \beta\right) \\ \mathbf{X}^{-} = \mathbf{X}^{m} + \varepsilon\, \mathbf{f}\left(\mathbf{X}^{m}, -\Delta L/2, \varepsilon, \alpha, \beta\right) \end{cases} \tag{12}$$

where $\mathbf{X} = (a, P_1, P_2, Q_1, Q_2)^T$. The superscript m indicates the value of the parameters at the mid-point, whereas $+$ and $-$ signs indicate forward and backward expansions, respectively.

B. Statement of the Algebraic Problem

In order to formulate a well-posed low-thrust Lambert problem for a specified transfer time ToF and a given set of boundary conditions for equinoctial parameters at initial and final time, the total number of unknowns must be equal to the number of equations. If the trajectory is discretized by means of n intervals, the system of $5n + 6$ algebraic equations achieves the form

$$\begin{cases} \mathbf{X}_1^- - \mathbf{X}_0 = 0 \\ \quad \dots \\ \mathbf{X}_{k+1}^- - \mathbf{X}_k^+ = 0 \\ \quad \dots \\ \mathbf{X}_n^- - \mathbf{X}_{n-1}^+ = 0 \\ \mathbf{X}_n^+ - \mathbf{X}_F = 0 \\ ToF = \sum_{k=1}^{n} \Delta t_k \end{cases} \tag{13}$$

where $\mathbf{X_0}$ and $\mathbf{X_F}$ are the prescribed initial and final values of 5 orbit parameters, respectively, and Δt_k is the time-of-flight for the k–th discretization arc estimated by means of the perturbative expansion. The set of algebraic equations is constituted by

- 5×2 boundary conditions on equinoctial elements;
- $5\,(n-1)$ continuity conditions for equinoctial elements at break points;
- 1 equation for the ToF.

The unknown quantities can be grouped into two classes:

- orbit parameters and, in particular, total trajectory angular travel ΔL_{tot} (given by $\sum_{k=1}^{n} \Delta L_k$) and $5n$ equinoctial variables at the mid–point of each discretization arc;
- control variables, that is magnitude of thrust T, azimuth and inclination, α and β.

Given the number of unknowns related to the values of orbit parameters at break-points, 5 control variables remain available for formulating a well posed algebraic problem, where the number of unknowns exactly matches the number of equations. Considering that the use of low-thrust is particularly convenient for varying orbit energy, the azimuth angle α is assumed constant and equal

to 90° most of the times, which implies that the in-plane component of thrust lies in the transverse direction, thus minimizing gravity losses [29]. When a change in orbit inclination or right ascension of the ascending node (RAAN) is required, an out-of-plane component of thrust is necessary. In this case, each revolution around the primary body is divided into two parts and thrust elevation β assumes different values along each half of a revolution, β_1 and β_2, in order to accomplish the required plane change. When a simultaneous change in inclination and RAAN is required, each revolution can be divided into four parts, with thrust angle switching between $\pm\beta_1$ and $\pm\beta_2$ along opposite quadrants, in order to maintain the same number of unknowns.

Note that, in a more general framework of optimal low-thrust transfers, it is possible to define a larger set of unkwons (e.g. different values of piecewise constant acceleration magnitude and angles over each trajectory arc), in order to minimize a desired performance index (e.g. total ΔV or transfer time). This is done in Ref. [18], where optimal maneuvers were derived by means of different discretization methods, including finite elements and the perturbative expansion described here in more detail.

For a three-dimensional maneuver, three unknowns for the acceleration profile $\varepsilon = T/m$ need to be defined. In what follows, ε is assumed constant along the first $n-2$ arcs. It is thus possible to exploit the last two discretization intervals, where ε is left free to vary, in order to match orbit parameters at arrival. This was proven to be the most critical task for the convergence of the numerical scheme adopted for the solution of the set of algebraic equations, Eq. (13). The assumption of constant acceleration throughout most of the transfer is not totally rigorous since vehicle mass decreases as it travels along its trajectory. Moreover, especially for long mission, as in the Earth-Mars case, the influence of secondary bodies should be considered. However, the assumption of constant acceleration modulus, without external disturbances forces, is acceptable for a preliminary analysis [13, 30, 31].

Only continuous thrusting cases are dealt with, without dealing with coasting arcs in the formulation described above. Coast arcs could be introduced at the beginning and/or at the end of the transfer, where the angular amplitude of the coast arc(s) substitutes one (or two) of the unknowns listed above, possibly the acceleration ε in the last (or in the last two) discretization arc.

As a final observation, note that a positive thrust in the transverse direction with $\alpha = 90$ deg allows for increasing orbit energy. When orbit energy needs to be decreased, a negative value of ε can be encountered (see as an example the results in Tab. 2 and Fig. 5.a.). Although conventionally a positive acceleration is always assumed and angle α reversed to -90 deg for decreasing energy, numerical convergence of the method proved to be easier, when ε was left free to smoothly vary between positive and negative values, rather than expecting the algorithm to capture a 180 deg discontinuous change in α.

C. Planar case

For the planar case the problem can be stated in slightly different (and to some extent, simpler) terms. When orbit plane is constant, 2 equinoctial parameters, namely Q_1 and Q_2, are no longer necessary and, as a consequence, their values are removed from the list of unknowns. The set of algebraic equations is thus made of $3\,(n+1)$ equations of continuity at break points plus the equation for the final time, ToF, for a total of $3n+4$ equations.

The unknown quantities are the total trajectory angular travel ΔL_{tot} and $3n$ equinoctial variables evaluated at the middle point of each discretization arc. In the planar case only 3 control variables are thus sufficient to make the problem well posed. It has been assumed that acceleration T/m remains constant for the first $n-2$ intervals and it can vary in the last two intervals, as in three-dimensional case. The angle α is assumed constant and equal to 90°, whereas β is obviously left equal to 0°.

D. Numerical aspects of the solution scheme

The system of algebraic equations represented by Eq. (13) is solved by means of a sequential-quadratic programming (SQP) method. A value of 10^{-7} was selected for termination tolerance on function value at convergence. The numerical scheme successfully finds the evolution of equinoctial variables from initial to final conditions in the prescribed time, total trajectory angular travel and thrust profile (modulus and inclination), starting from a first guess solution.

As it is often the case with many numerical schemes, the identification of a suitable first guess

can play a fundamental role on the convergence of the algorithm, in terms of capabilities of finding a solution and/or computational effort for reaching convergence. Numerical performance are sensitive to the initial guess and total trajectory angular travel and acceleration magnitude proved to be the most critical parameters. In this respect, if thrust magnitude lies in a range which makes the prescribed transfer far from feasible, convergence to a solution can be hindered. E.g., for planar orbit transfers with relevant variations of the semi-major axis, a_0, a good initial guess is provided by constant thrust profile which enables to cover the specific orbital energy gap $\Delta\mathcal{E} = \mathcal{E}_F - \mathcal{E}_0$ between the initial (0) and final (F) orbit in the prescribed time ToF, where $\Delta\mathcal{E} = -\mu/(2a_F) + \mu/(2a_0)$. Once an initial guess is available, the numerical scheme demonstrates good convergence capabilities, as less than 20 iterations are usually sufficient for reaching convergence. Once a solution is obtained, it is possible to exploit it for performing systematic parametric studies for different transfer scenarios by changing problem parameters one at the time, thus mitigating the issue of identifying suitable initial guesses for the algorithm.

A detailed analysis of CPU time is not performed here, because of the wide variation of numerical performance in terms of number of iterations needed for reaching convergence, which depends on the particular test case considered and the quality of the initial guess. The number of iterations for convergence can be as low as 3 or 4 in some cases. Anyway, the CPU time remains small (few seconds) also in those cases when more iterations are needed (15 to 20 iterations, in some cases), if the numerical quadrature of the integrals required for the determination of t_{12} is not performed and the term t_{12} dropped in the estimate of total time of flight, as suggested in subsection II.D.

Note that, at this point, a comparison with optimization tools is not a fair one, when one considers that only constraint enforcement (continuity and time of flight) is required by the present technique. An analysis of numerical performance in terms of CPU time was performed in [18], where both the computational cost of a propagation based on the perturbative expansion and the total time required for optimizing a whole maneuver, discretizing it by means of centered perturbative expansion, were performed.

Table 1 Case 1: initial and final orbit parameters for the Earth-Mars transfer

Parameter	Symbol	Initial	Final	Units
Semi-major axis	a	$1.49 \cdot 10^8$	$2.28 \cdot 10^8$	km
Eccentricity	e	0.01	0.093	
Argument of perigee	ω	120	-70	deg
True anomaly (case A)	θ	0	22.7	deg
True anomaly (case B)	θ	0	-125.4	deg

IV. Results

In order to demonstrate the use of perturbative expansions in the solution of the low-thrust Lambert problem, three cases were considered. Case 1 is a planar transfer from Earth to Mars. In Case 2, a planar multi-revolution transfer from a low-Earth orbit (LEO) to International Space Station ISS orbit is dealt with, which requires an increase in orbit altitude of 95 km. Finally Case 3 is represented by an orbit transfer from GTO (Geostationary Transfer Orbit) to HEO (Highly Elliptical Orbit), which requires a 116° change in orbit plane inclination. Cases 1 and 2 are very similar to two mission scenarios considered in [18], in order to obtain reasonable data for a feasible transfer by means of a low-thrust propulsion system. Case 3 was created to prove the viability of the method for a demanding three-dimensional maneuver with a large orbit inclination change.

A. Earth-Mars transfer

For the Earth-Mars transfer (Case 1), the trajectory is divided into 20 arcs. The initial guess for the SQP iterative procedure is a constant acceleration profile with magnitude $\varepsilon = 1.2 \cdot 10^{-4}$ m/s^2, equivalent to a thrust of 0.12 N applied to a spacecraft with a mass of 1000 kg. For this planar case, thrust azimuth α and elevation β are set at 90° and 0°, respectively, as outlined in the previous section. The boundary values for the low-thrust Lambert problem are presented in Tab. 1 in terms of classical orbital parameters. The initial and final set of equinoctial variables are then obtained by applying Eq. (1).

The time of flight was selected considering a Hohmann transfer as a reference transfer orbit.

Table 2 Earth-Mars transfer results

Unknown	**Value**		**Units**
	Case 1.A	Case 1.B	
ΔL_{tot}	4π	3.3π	rad
ε_k, $k = 1, 2, \ldots, n-2$	$2.1487 \cdot 10^{-4}$	$1.671 \cdot 10^{-4}$	m/s^2
ε_{n-1}	$-2.2773 \cdot 10^{-4}$	$6.115 \cdot 10^{-4}$	m/s^2
ε_n	$-2.7364 \cdot 10^{-4}$	$5.855 \cdot 10^{-4}$	m/s^2

It is well known that this is the minimum–fuel maximum–time impulsive transfer between two circular coplanar orbits, with a double-tangent ellipse and two impulsive velocity changes [29]. In the low-thrust case the time required to complete the mission is necessarily higher, as the thrust is continuous but small. A transfer time ToF equal to 4.5 times Hohmann transfer duration was selected (Case 1.A). For the Earth-Mars transfer this implies a mission duration of 1162 days. This value is similar to that obtained in Ref. [18] for an optimal transfer of 1065 days, featuring an on-off structure of thrust profile and a maximum value of non-dimensional thrust modulus equal to $2.5 \cdot 10^{-4}$.

The algorithm converges after 9 iterations. Table 2 reports data for the solution found, that is, values of total trajectory angular travel ΔL_{tot}, thrust modulus ε in the first $n-2$ and in the last two intervals. The value of $\Delta L_{tot} = 4\pi$ leads to two complete revolutions, as shown in Fig. 4.

The evolution of equinoctial variables and classical orbit parameters is shown in Figs. 5 and Fig. 6, respectively. The semi-major axis increases monotonically in the first $n-2$ arcs and decreases in the last part of the trajectory in order to match the final position in the prescribed time. The continuity of equinoctial parameters P_1, P_2 is respected along the entire trajectory. These parameters show a periodic component during the continuous thrusting mission.

In order to assess the accuracy of the perturbative method, the results obtained are compared with a numerical solution, determined by means of Encke's method [29], using the values of α, β and ε found from the discretized solution of the low-thrust orbit transfer problem. The numerical propagation in time is stopped when the total angular travel is equal to ΔL_{tot}. The relative error

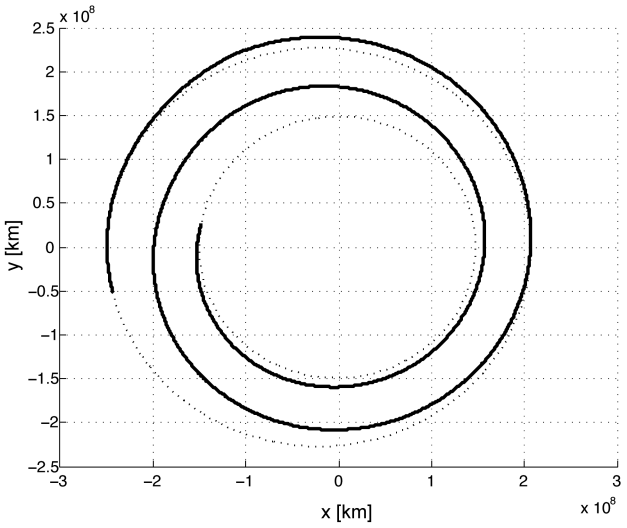

Fig. 4 Earth-Mars low-thrust trajectory for Case 1.A (1162 days transfer).

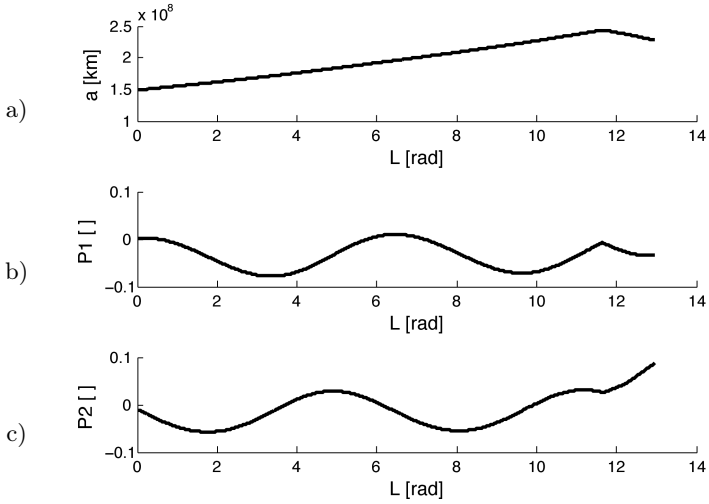

Fig. 5 Evolution of equinoctial variables for Earth-Mars low thrust trajectory (Case 1.A): semi-major axis (a), P_1 (b), and P_2 (c).

between the two solution is then evaluated as a function of L.

Figure 7 shows that the maximum value of the relative error $\Delta r/r$ is less than $6.7 \cdot 10^{-4}$. This is a good result, considering also that the value of the non-dimensional thrust parameter $\hat{\varepsilon}$ is rather large. Note that during the initial phase, a larger error is reached at the center of each discretization arc. More significant discrepancies between the accurate numerical solution and the approximate trajectories based on perturbative expansions slowly grows along the trajectory. At the end of the orbit transfer the error increases more significantly for the last two discretization arcs, because of (i) the effects of the overall error build-up and (ii) because of the higher values of the thrust required

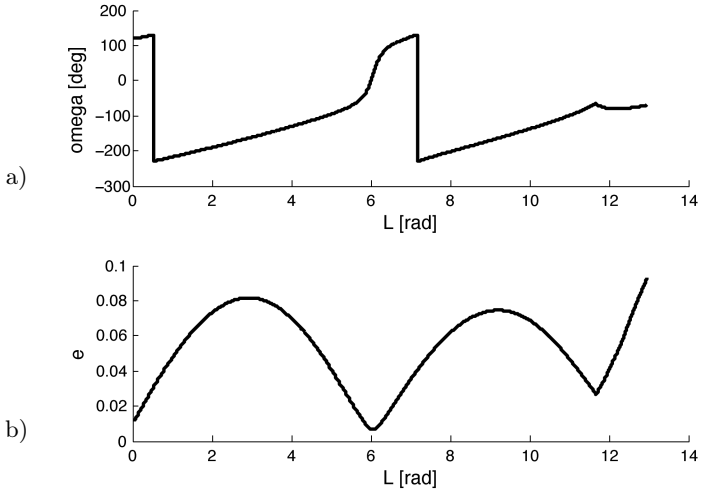

Fig. 6 Evolution of longitude of the ascending node (a) and eccentricity (b) for Earth-Mars low thrust trajectory (Case 1.A).

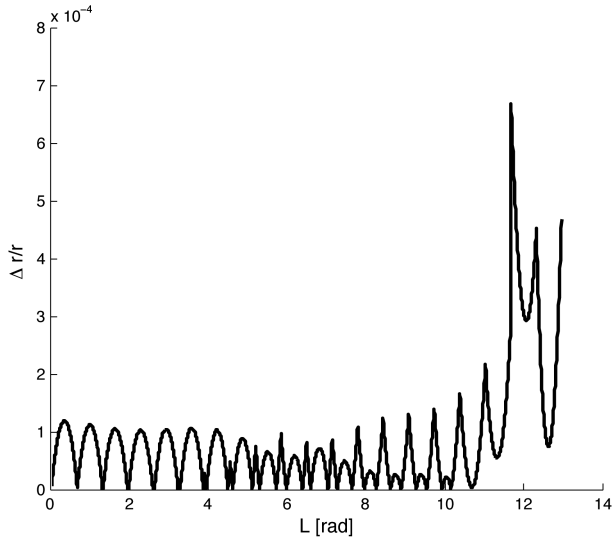

Fig. 7 Position error for Earth-Mars low-thrust trajectory (Case 1.A).

in the final part of the trajectory to correctly match the final desired position. Nonetheless, the accuracy appears acceptable for preliminary mission design.

Provided that a overshoots its desired value during the first $n-2$ trajectory element, a negative thrust is required to decrease orbit energy. This result is not surprising, when one considers that the problem is formulated as a boundary value one, and there is no optimization process involved. This means that the numerical procedure is simply required to match the prescribed boundary conditions (together with continuity of orbit elements at the break points), regardless of considerations on fuel (or equivalently ΔV) and/or transfer time optimality, the latter being assigned *a priori*, as in the

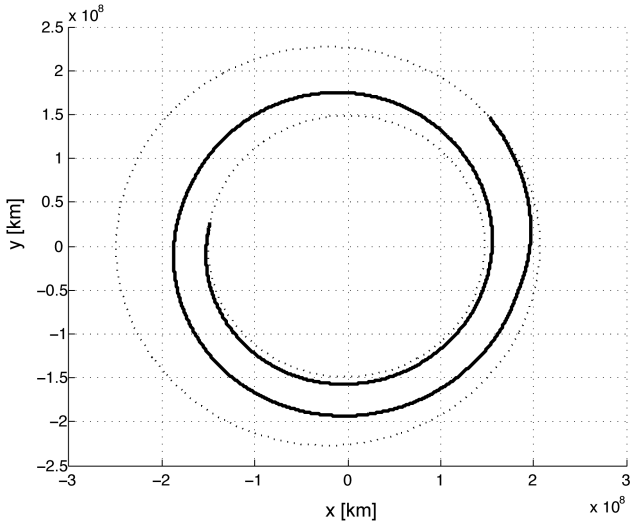

Fig. 8 Earth-Mars low-thrust trajectory for Case 1.B (775 days transfer).

classical Lambert problem for ballistic transfers.

At the same time, this solution method lends itself for an efficient analysis of possible transfer trajectories. As an example, if transfer time is reduced to 775 days (Case 1.B), the trajectory obtained is reported in Fig. 8, corresponding to a different evolution of orbit parameters over little more than 1.5 revolutions (Fig. 9). The results for this second Earth-Mars transfer are reported in the third column of Table 2. This second solution results into a semi-major axis monotonically increasing. In this case the value of ε in the first $n-2$ segments is smaller, compared with that derived for the longer transfer time, whereas ε increases significantly in the last two arcs, for correctly phasing the spacecraft on its final orbit at the prescribed time. Note that the last two arcs are covered in a longer time. As a consequence, the variation of the total time of flight is more sensitive to the values of ε in this last two portions of the trajectory, which become critical in order to match the desired value of ToF.

The error with respect to an accurate numerical solution obtained for the values of continuous thrust reported in the last column of Table 2 shows a similar pattern, with respect to that obtained for the previous example (Fig. 10), for the first $n-2$ discretization arcs. The increase in the perturbation parameter $\varepsilon = T/m$ required over the last two segments causes a significant error in the estimate of the position along the arc, but it does not causes major problems at discretization bounds, that is, the final position is predicted with a reasonable accuracy.

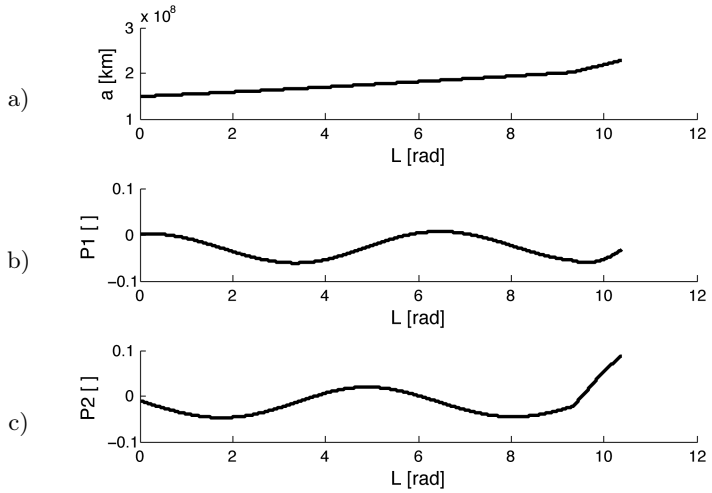

Fig. 9 Evolution of equinoctial variables for Earth-Mars low thrust trajectory (Case 1.A): semi-major axis (a), P_1 (b), and P_2 (c).

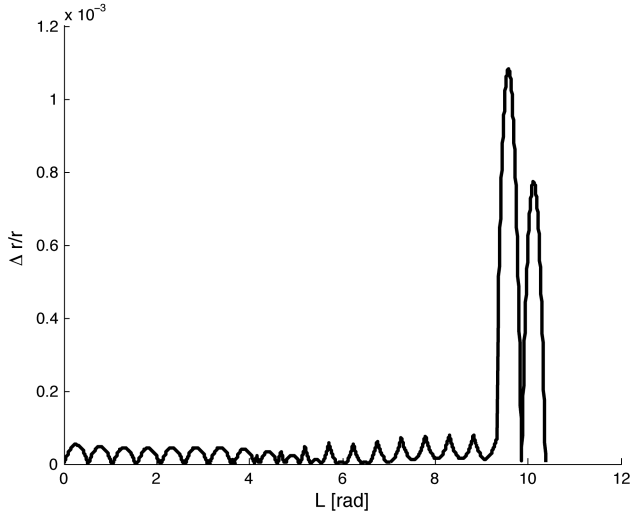

Fig. 10 Position error for Earth-Mars low-thrust trajectory (Case 1.B).

B. LEO altitude increase

Case 2 deals with a transfer that requires a semi-major axis increase of 95 km. The initial LEO corresponds to a typical injection altitude obtained from an Ariane 5 launcher, with an initial radius of 6640 km, whereas the final orbit corresponds to the International Space Station circular orbit, with a radius equal to 6735 km. All the remaining orbit elements are assumed equal for the initial and final orbits (Tab. 3). The time of flight for the low-thrust Lambert problem is assumed equal to 2.02 days (64 times the ToF required for a Hohmann transfer between the same orbits), that is, equal to the result proposed in [18] for an optimal minimum ΔV transfer between the same orbits.

Table 3 Case 2: initial and final orbit parameters for LEO altitude increase

Parameter	Symbol	Initial value	Final value	Units
Semi-major axis	a	6640	6735	km
Eccentricity	e	0.001	0.001	
Inclination	i	0.05	0.05	deg
RAAN	Ω	240	240	deg
Argument of perigee	ω	10	10	deg
True anomaly	θ	0	0	deg

Table 4 LEO altitude increase results

Unknown	Value	Units
ΔL_{tot}	64π	rad
ε_k, $k = 1, 2, \ldots, n-2$	$3.1763 \cdot 10^{-7}$	m/s^2
ε_{n-1}	$3.7419 \cdot 10^{-7}$	m/s^2
ε_n	$3.7250 \cdot 10^{-7}$	m/s^2

Initial and final orbits are coplanar, as in Case 1. Thrust elevation β is consequently assumed zero and thrust azimuth α is set at 90°, which is a transverse direction close to the tangent to the trajectory. The discretization of the low-thrust Lambert problem follows the pattern outlined in the previous section for planar cases. The trajectory is discretized with 64 elements of equal ΔL and the initial guess is a constant thrust profile with magnitude $\varepsilon = 10^{-7}$ m/s^2, equivalent to a thrust of 1 mN applied to a spacecraft with 10000 Kg of mass.

The algorithm converges after 4 iterations. The values of thrust modulus ε are reported in Table 4. The total trajectory angular travel ΔL_{tot} is 64π, that leads to 32 revolutions, as shown in Fig. 11. Figure 12 shows the evolution of equinoctial parameters. Semi-major axis has a linear increase along the entire trajectory. The plots of P_1 and P_2 have a periodic component due to continuous thrust along the multi-revolution trajectory. The comparison with the numerical solution obtained from orbit propagation with Encke's method (omitted for the sake of conciseness) shows

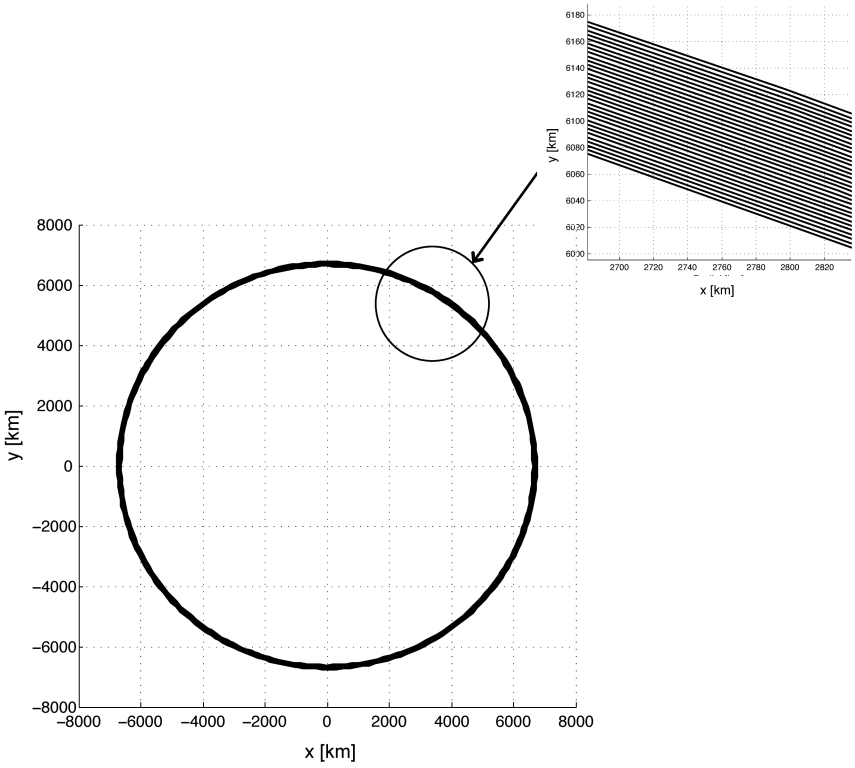

Fig. 11 Multi-revolution low-thrust trajectory for LEO altitude increase (Case 2).

that the perturbative approach provides a very accurate solution for these small values of ε, the maximum relative error being less than $6 \cdot 10^{-9}$. This confirms that the error strongly dependends on perturbation parameter ε, increasing superlinearly with it.

C. HEO transfer trajectory.

The third test case is an Earth transfer from a geostationary transfer orbit (GTO) to a highly elliptical orbit (HEO) involving a large plane change of 115.94 degrees. This is the most complicated transfer since it requires a three-dimensional maneuver with simultaneous variations of semi-major axis and eccentricity in addition to a large inclination change. Argument of perigee and longitude of the ascending node are maintained constant while the other orbit elements are driven to their final values.

The boundary conditions expressed in terms of classical orbit elements are reported in Tab. 5. A desired transfer time equal to 14 days is considered. In this case the trajectory is discretized by means of 120 finite equiangular arcs, with $\Delta L_k = 90$ deg. The initial guess is a constant thrust

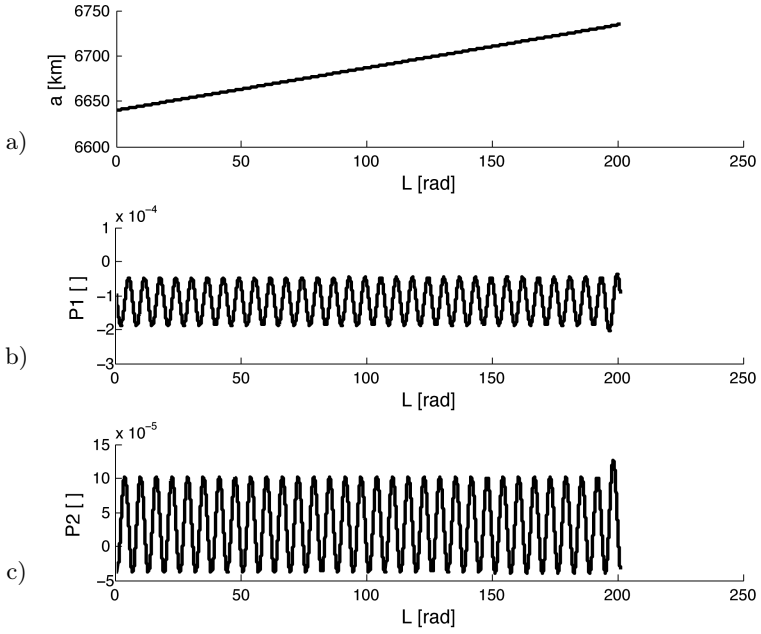

Fig. 12 Evolution of equinoctial variables for low-thrust LEO altitude increase (Case 2): semi-major axis (a), P_1 (b), and P_2 (c).

Table 5 Case 3: initial and final orbit parameters for HEO transfer.

Parameter	**Symbol**	**Initial value**	**Final value**	**Units**
Semi-major axis	a	24505.9	26500	km
Eccentricity	e	0.725	0.700	
Inclination	i	0.06	116	deg
RAAN	Ω	180	180	deg
Argument of perigee	ω	180	180	deg
True anomaly	θ	0	0	deg

profile with magnitude $\varepsilon = 1 \cdot 10^{-2}$ m/s^2, equivalent to a thrust of 100 N applied to a spacecraft with a mass of 10000 kg.

Thrust azimuth α was set at 90° , whereas thrust modulus ε and elevation β are determined from the solution of the set of algebraic conditions outlined in the previous section. The algorithm convergences in 15 iterations. The transfer requires 30 revolutions, as shown in Fig. 13. The values of thrust magnitude and elevation over the orbit plane determined at convergence are reported in Table 6. The evolution of equinoctial variables is presented in Fig. 14, whereas Fig. 15 shows

Table 6 HEO transfer results

Unknown	Value	Units
ΔL_{tot}	60π	rad
ε_k, $k = 1, 2, \ldots, n-2$	$1.07 \cdot 10^{-2}$	m/s^2
ε_{n-1}	$2.53 \cdot 10^{-2}$	m/s^2
ε_n	$15.4 \cdot 10^{-2}$	m/s^2
β_1	14.2	deg
β_2	13.7	deg

the variation of eccentricity and inclination along the orbit. The plots indicate that the algorithm successfully identifies a maneuver that drives the orbit parameters to their final desired values almost monotonically.

The comparison with the numerical solution (Fig. 16) shows that the error is larger than in previous test cases. This is caused by the value of the non-dimensional perturbation parameter, which becomes two order of magnitude higher. Moreover, also the size of the discretization true longitude increments is relatively large. However the maximum relative error along the orbit and on the final position is less than 0.0035. Thus, perturbative expansion exhibits a reasonable accuracy also for a transfer case with relatively high thrust and large plane changes. Moreover, it should be noticed that the error expressed in terms of absolute position is a particularly severe index. Table 7 reports the maximum relative error for equinoctial parameters, showing that the maximum relative error affects Q_2. Error on the evaluation of semi-major axis is 0.035%, which is also a good result for a first order approximation method with high values of thrust acceleration.

D. Trajectory Element Discretization

In the results presented above, the whole trajectory was discretized by means of elements with constant angular amplitude in terms of true longitude increments. Provided that the error grows superlinearly for higher values of non-dimensional acceleration $\hat{\varepsilon}$ [18], reducing the size of the discretization increment of the angular travel as the spacecraft moves away from the primary body

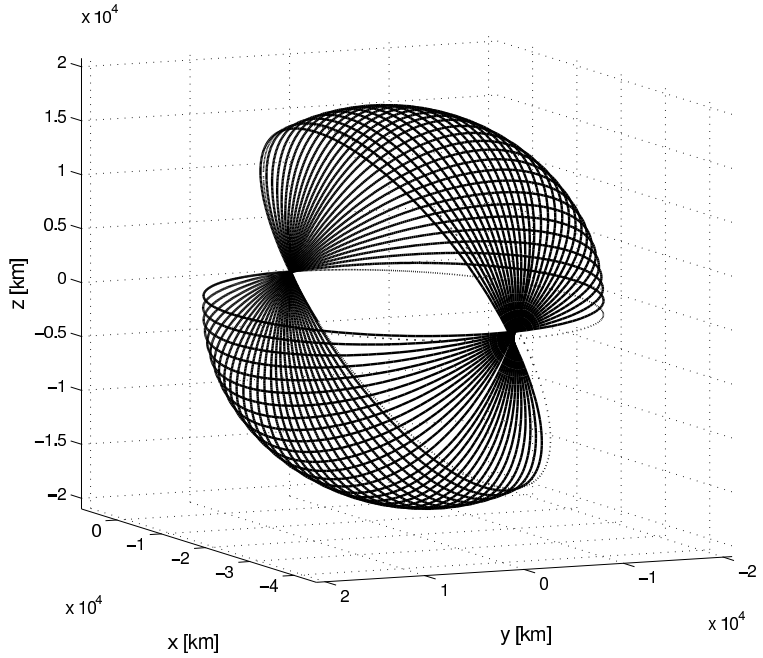

Fig. 13 HEO trajectory.

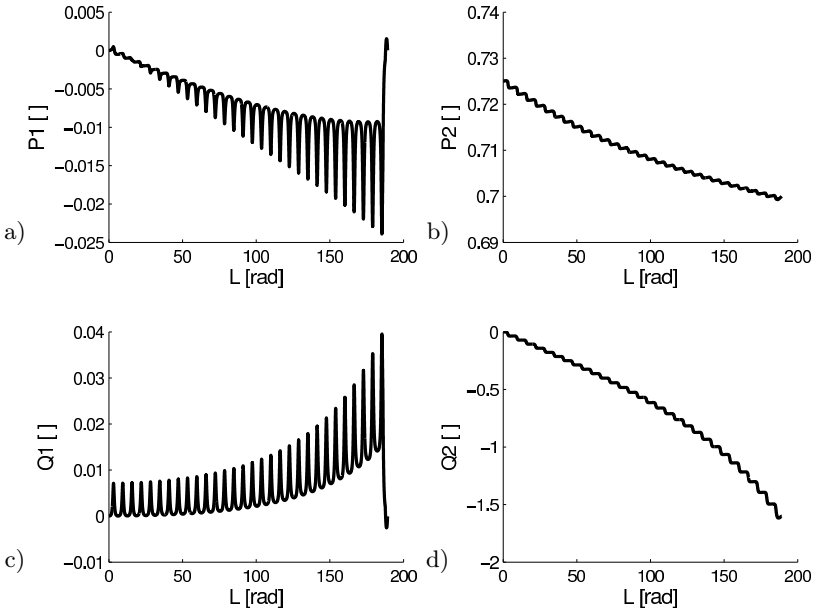

Fig. 14 Evolution of equinoctial variables for transfer to HEO (Case 3): P_1 **(a),** P_2 **(b),** Q_1 **(c), and** Q_2 **(d).**

appears as a reasonable attempt for reducing the error introduced by the perturbative expansion in the solution of the low-thrust Lambert problem. A logarithmic law is employed for increasing the number of arcs in the last portion of the trajectory, farther away from the primary body, while

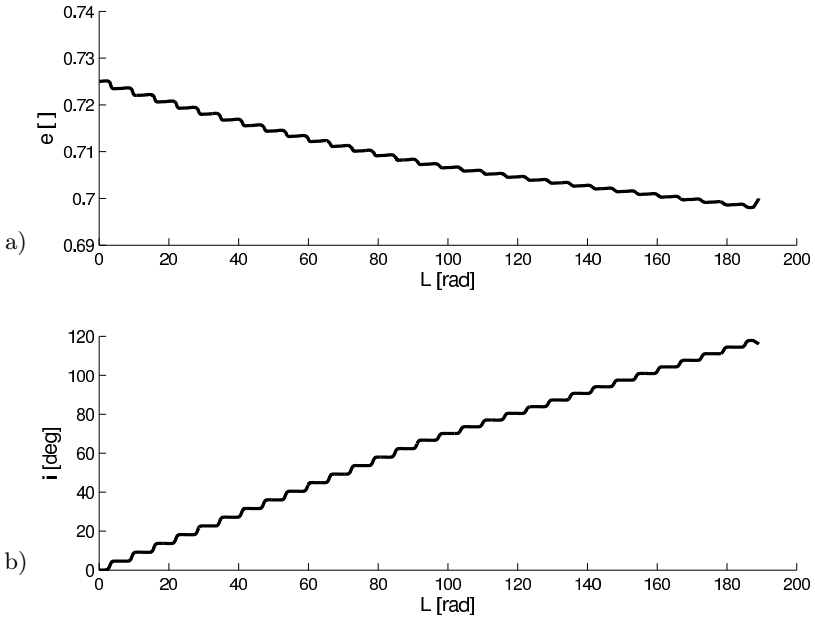

Fig. 15 Evolution of eccentricity (a) and inclination (b) for transfer to HEO (Case 3).

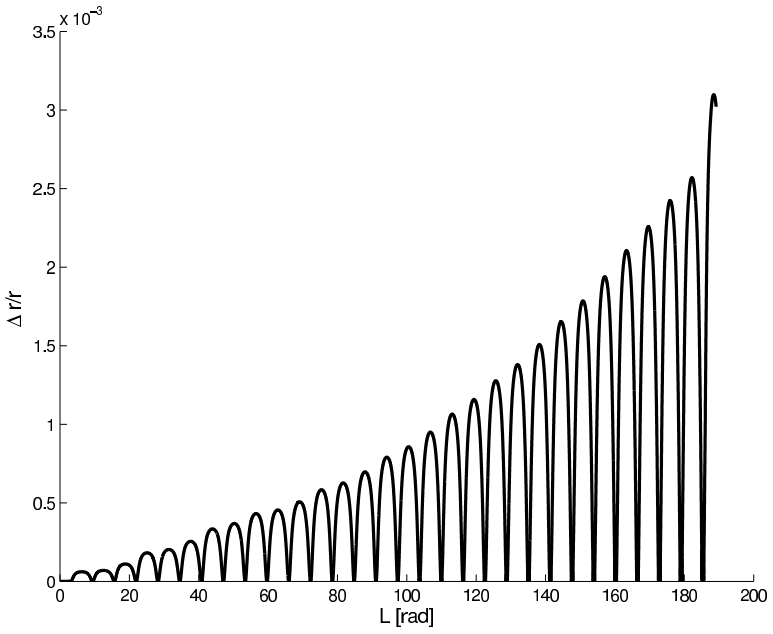

Fig. 16 Position error for low-thrust transfer to HEO (Case 3).

Table 7 HEO transfer: error on equinoctial parameters.

Equinoctial parameter	Maximum error
a	0.030 %
P_1	0.50 %
P_2	0.093 %
Q_1	0.68 %
Q_2	1.84 %

increasing their amplitude in the first portion of the transfer, closer to the primary body, where $\hat{\varepsilon}$ is smaller, thanks to the increased value of the local gravity acceleration, and smaller errors are expected.

Using as a reference value a uniform spacing for the increments of true longitude, such that $\Delta L_{ref} = \Delta L_{tot}/n$, where n is the total number of arcs along the trajectory, the arc segments are logarithmically spaced between decades $\Delta L_{ref}\ 10^a$ and $\Delta L_{ref}\ 10^b$, when $\Delta L_k = \Delta L_{ref} \cdot 10^{[a+(k-1)(b-a)/(n-1)]}$. The bounds a and b for the spacing law are selected in order to reduce the size of the angular travel increment by 25% at the end of the trajectory. This choice is the result of a trade-off between reducing the value of ΔL_k for the final segments, without making them too short (thus hindering convergence, because of a reduced sensitivity of the residuals to the final values of ε_k for $k = n-1$ and n)), while avoiding an excessive growth of the angular travel for the initial arcs, that would results in a fast growth of the error at the beginning of the maneuver.

This discretization approach was applied for all the test cases presented above. As an example, errors in the position for the Earth-Mars mission discretized by means of the logarithmic law (Case 1.C) are shown in Fig. 17. The relative error is reduced with respect to that obtained for uniform discretization, but the improvement appears to be rather small, at least for the considered variation of orbit radius.

Similar results are obtained also for the other test cases (not reported for the sake of conciseness), thus showing that, although always better, a logarithmic distribution of discretization increments of true longitude does not allow for major improvements in the overall accuracy of the solution. The

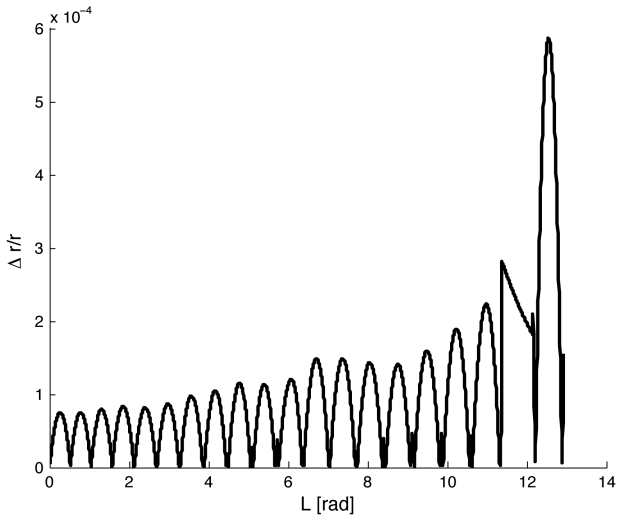

Fig. 17 Position error for Earth-Mars low-thrust trajectory with logarithmic variation of discretization angular travel (Case 1.C).

reason for such a modest gain is still related to the characteristics of the error on a single arc, as the gain in accuracy for the last elements of the discretization is partially spoilt by the increase in arc size for the initial portion of the transfer.

Accuracy is significantly improved over the entire trajectory only by increasing the number n of discretization arcs. As an example, when 40 elements are used for discretizing the trajectory (that is, twice as much those used for Case 1.A, B, and C), the error is reduced by almost one order of magnitude, at the expenses of a considerably higher computational cost, provided that an algebraic system with as many as 206 equations and unknowns need to be solved. In this latter case, the CPU time increases approximately by a factor 4.

V. Conclusions

The paper discusses a novel formulation for the so called low-thrust Lambert problem, stated in terms of a boundary value problem for equinoctial orbit parameters. The approach employs perturbative expansions of equinoctial variables for representing the evolution of orbit parameters along a low-thrust transfer arc, where the perturbative parameter is given by the magnitude of thrust acceleration. First order expansions applied to Gauss variational equations for finite arc elements are employed to discretize the orbit transfer between two prescribed initial and final orbits. An

implicit algebraic problem is obtained, that enforces the desired time of flight between the orbits. The solution provides simultaneously the characteristics of the trajectory and thrust magnitude and direction that result into the desired orbit transfer, without the need for any *a priori* assumption on orbit shape. The price to pay is the need for a numerical solution of a set of algebraic equations obtained from the discretization of the transfer trajectory. This set of equation can become rather large for long multi-revolution cases.

The discretized perturbative approach was applied to three test cases (an Earth-Mars transfer, a multiple revolution altitude increase and a GTO-HEO transfer), proving the viability of the approach for both in-plane orbit transfer and maneuver requiring large inclination changes. Accuracy of the solution was investigated in all these cases, comparing the results obtained from the perturbative expansion with those derived by means of accurate numerical orbit propagation. A significant effect of true longitude increment and perturbation parameter was highlighted. For smaller values of non-dimensional perturbation parameter the results remain accurate also for very long, multi-revolution transfers, whereas accuracy rapidly decreases when higher values of thrust magnitude are necessary. Nonetheless, the solution derived still suits a preliminary parametric mission analysis.

References

[1] J. Schoenmaekers, "Post-launch optimisation of the Smart-1 low-thrust trajectory to the Moon," *Proceeding of the 18th International Symposium on Space Flight Dynamics*, ESA Special Publication, Vol. 548, Noordwijk, The Netherlands, 2004, pp. 505-510.

[2] K. Uesugi, "Space engineering spacecraft (Muses) program in ISAS featuring its latest mission Hayabusa," *Proceedings of International Conference on Recent Advances in Space Technologies*, Vol. 12, 1999, pp. 451-484; doi: 10.1109/RAST.2003.1303961

[3] M. Novara, "The Bepicolombo esa cornerstone mission to Mercury," *Acta Astronautica*, Vol. 51, 2002, pp. 387-395; doi:10.1016/S0094-5765(02)00065-6

[4] G. Li, Z. Yi, G. Heinzel, A. Rüdiger, O. Jennrich, L. Wang, Y. Xia, F. Zeng, Z. Haibin, "Methods for orbit optimization for the LISA gravitational wave observatory," *International Journal of Modern Physics D*, Vol. 17 , No. 7, 2008, pp. 1021-1042; doi: 10.1142/S021827180801267X

[5] G. Yang, "Direct optimization of low-thrust many-revolution Earth-orbit transfers," *Chinese Journal of Aeronautics*, Vol. 22, No. 4, 2009, pp. 426-433; doi: 10.1016/S1000-9361(08)60121-1

[6] R. H. Battin, *An Introduction to the Mathematics and Methods of Astrodynamics Revised Edition*, AIAA Education Series, 1999, Chaps. 6-7.

[7] K.F. Gauss, *Theoria Motus Corporum Coelestium in Sectionibus Conicis Solem Ambientium*, edited by F. Perthes and I. H. Besser, 1809; English translation by C. H. Davis, *Theory of the Motion of the Heavenly Bodies Moving About the Sun*, Little, Brown and Co., Boston, 1857.

[8] H. Shen, P. Tsiotras, "Using Battin's method to obtain multiple-revolution Lambert's solution," AAS paper 03-568, in *Advances in Astronautical Sciences*, Vol. 116, Univelt Inc., San Diego (CA), 2004, pp. 1067-1084.

[9] M. Bando, H. Yamakawa, "A new Lambert algorithm using the Hamilton-Jacobi-Bellman equation," *Journal of Guidance Control, and Dynamics*, Vol. 33, No. 3, 2010, pp. 1000-1008.

[10] L. A. Loechler, *An elegant Lambert algorithm for multiple revolution orbits*, M.Sc. thesis, Massachusetts Institute of Technology, 1988.

[11] G. Avanzini, "A simple Lambert algorithm," *Journal of Guidance, Control, and Dynamics*, Vol. 31, No. 6, 2008, pp. 1587-1594; doi: 10.2514/1.46751

[12] G. Lantoine, and R.P. Russell, "Complete, Closed-Form Solutions of the Stark Problem," *Celestial Mechanics and Dynamical Astronomy*, Vol. 109, No. 4, 2011, pp. 333-366, doi: 10.1007/s10569-010-9331-1.

[13] A. E. Petropoulos, J. M. Longuski, "Shape-based algorithm for automated design of low-thrust, gravity assist trajectories," *Journal of Spacecraft and Rockets*, Vol. 41, No. 5, September-October 2004, pp. 787-796; doi: 10.2514/1.13095

[14] A. E. Petropoulos, J. M. Longuski, "A review of some exact solutions to the planar equations of motion of a thrusting spacecraft," in *Proceeding of the 2$^{\text{nd}}$ International Symposium on Low Thrust Trajectories*, Toulouse, France, 2002.

[15] E. Vellutini, and G. Avanzini, "Shape-Based Design of Low-Thrust Trajectories to Cislunar Lagrangian Point," *Journal of Guidance, Control, and Dynamics*, Vol. 37, No 4, 2014, pp. 1329-1335; doi: 10.2514/1.G000165.

[16] D. Izzo, "Lambert's Problem for Exponential Sinusoids," *Journal of Guidance, Control, and Dynamics*, Vol. 29, No. 5, 2006, pp. 1242-1245. doi: 10.2514/1.21796

[17] M. Vasile, O. Schutze, O. Junge, G. Radice, M. Dellnitz, D. Izzo, "Spiral trajectories in global optimization of interplanetary and orbital transfers," ESA, Final Report ACT-RPT- ARI-05-4106, 2006.

[18] F. Zuiani, M. Vasile, A. Palmas, and G. Avanzini, "Direct transcription of low-thrust trajectories with finite trajectory elements," *Acta Astronautica*, Vol. 72, 2012, pp. 108-120; doi:

10.1016/j.actaastro.2011.09.011

[19] F. Zuiani, and M. Vasile, "Extension of Finite Perturbative Elements for Multi-Revolution, Low-Thrust Propulsion Transfer Optimisation", 63rd International Astronautical Congress, Paper IAC-12-C1.4.6, Naples, Italy, 1-5 October, 2012.

[20] J. Sims, P. Finlayson, E. Rinderle, M. Vavrina, T. Kowalkowski, "Implementation of a Low-Thrust Trajectory Optimization Algorithm for Preliminary Design," AAS/AIAA Astrodynamics Specialist Conference, AAS Paper 2006-6746, Keystone, Colorado, August 21-24, 2006.

[21] Y. Gao. "Low-Thrust Interplanetary Transfers, Including Escape and Capture Trajectories", *Journal of Guidance, Control, and Dynamics*, Vol. 30, No. 6, 2007, pp. 1814-1818. doi: 10.2514/1.26427

[22] Press,W.H., Flannery,B.P., Teukolsky,S.A., and Vetterling,W.T., *Numerical Recipes - The Art of Scientific Computing*, Cambridge Univ. Press, Cambridge, England, UK, 1986, pp. 77-101.

[23] P.J. Enright, and B.A. Conway,"Optimal finite-thrust spacecraft trajectories using collocation and nonlinear programming", *Journal of Guidance, Control, and Dynamics*, Vol. 14, No. 5, 1991, pp. 981-985; doi: 10.2514/3.20739

[24] S. Tang, and B.A. Conway, "Optimization of low-thrust interplanetary trajectories using collocation and nonlinear programming", *Journal of Guidance, Control, and Dynamics*, Vol. 18, No. 3, 1995, pp. 599-604; doi: 10.2514/3.21429

[25] E. Roth, "The Gaussian form of the variation of parameter equations formulated in equinoctial elements - applications: Airdrag and radiation pressure," Acta Astronautica, Vol. 12, No. 10, 1985, pp. 719-730; doi: 10.1016/0094-5765(85)90088-8

[26] J. Kevorkian, J. Cole, *Multiple Scale and Singular Perturbation Methods*, Springer, New York, 1996, Ch. 2.

[27] R. Johnson, *Singular Perturbation Theory*, Springer, Boston, 2005, Ch. 2.

[28] A. Palmas, *Approximations of low-thrust arcs by means of perturbative approaches*, Master's thesis, Politecnico di Torino, 2010.

[29] R. Bate, D. Mueller, J. White, *Fundamentals of Astrodynamics*, Dover Publications Inc, New York, 1971.

[30] A.E. Petropoulos, "Simple Control Laws for Low-Thrust Orbit Transfer," AAS/AIAA Astrodynamics Specialist Conference, AAS Paper 2003-630, Big Sky, Montana, August 3-7, 2003.

[31] J. A. Sims, N. Flanagan, "Preliminary design of low-thrust interplanetary missions," AAS paper 99-338, in *Advances in Astronautical Sciences*, Vol. 103, Univelt Inc., San Diego (CA), 2000, pp. 583-592.

Appendix

$$
\begin{aligned}
I_{11}(L) &= \int_{L_0}^{L} \frac{1}{(1+P_{10}\sin L+P_{20}\cos L)}\,dL \\
I_{12}(L) &= \int_{L_0}^{L} \frac{1}{(1+P_{10}\sin L+P_{20}\cos L)^2}\,dL \\
I_{13}(L) &= \int_{L_0}^{L} \frac{1}{(1+P_{10}\sin L+P_{20}\cos L)^3}\,dL \\
I_{s2}(L) &= \int_{L_0}^{L} \frac{\sin L}{(1+P_{10}\sin L+P_{20}\cos L)^2}\,dL \\
I_{s3}(L) &= \int_{L_0}^{L} \frac{\sin L}{(1+P_{10}\sin L+P_{20}\cos L)^3}\,dL \\
I_{s5}(L) &= \int_{L_0}^{L} \frac{\sin L}{(1+P_{10}\sin L+P_{20}\cos L)^5}\,dL \\
I_{c2}(L) &= \int_{L_0}^{L} \frac{\cos L}{(1+P_{10}\sin L+P_{20}\cos L)^2}\,dL \\
I_{c3}(L) &= \int_{L_0}^{L} \frac{\cos L}{(1+P_{10}\sin L+P_{20}\cos L)^3}\,dL \\
I_{c5}(L) &= \int_{L_0}^{L} \frac{\cos L}{(1+P_{10}\sin L+P_{20}\cos L)^5}\,dL
\end{aligned}
\tag{14}
$$

$$
\begin{aligned}
\Phi_{12}(L) &= -\frac{2}{\sigma}\left(\frac{1}{\sqrt{\sigma}}\arctan\frac{\frac{(P_{20}-1)\sin L}{\cos L+1}-P_{10}}{\sqrt{\sigma}}+\right. \\
&+ \left.\frac{\frac{(P_{10}^2+P_{20}^2-P_{20})\sin L}{\cos L+1}+P_{10}}{-(P_{20}-1)^2\frac{\sin^2 L}{(\cos L+1)^2}+2P_{10}(P_{20}-1)\frac{\sin L}{\cos L+1}+(P_{20}^2-1)}\right) \\
\Phi_{s2}(L) &= \frac{2}{\sigma}\left(\frac{P_{10}}{\sqrt{\sigma}}\arctan\frac{\frac{(P_{20}-1)\sin L}{\cos L+1}-P_{10}}{\sqrt{\sigma}}-\right. \\
&+ \left.\frac{\frac{P_{10}\sin L}{\cos L+1}+P_{20}+1}{-(P_{20}-1)\frac{\sin^2 L}{(\cos L+1)^2}+2P_{10}\frac{\sin L}{\cos L+1}+(P_{20}+1)}\right) \\
\Phi_{c2}(L) &= \frac{2}{\sigma}\left(\frac{P_{20}}{\sqrt{\sigma}}\arctan\frac{\frac{(P_{20}-1)\sin L}{\cos L+1}-P_{10}}{\sqrt{\sigma}}-\right. \\
&+ \left.\frac{\frac{\sigma\sin L}{\cos L+1}-P_{10}P_{20}}{-(P_{20}-1)^2\frac{\sin^2 L}{(\cos L+1)^2}+2P_{10}(P_{20}-1)\frac{\sin L}{\cos L+1}+(P_{20}^2-1)}\right) \\
\Phi_{13}(L) &= \frac{2}{\sigma^2}\left(\frac{P_{20}^2+P_{10}^2+2}{\sqrt{\sigma}}\arctan\frac{\frac{(P_{20}-1)\sin L}{\cos L+1}-P_{10}}{\sqrt{\sigma}}+\right. \\
&+ [(P_{20}^4+2P_{20}^3+3P_{10}^2P_{20}^2-7P_{20}^2+2P_{10}^2P_{20}+4P_{20}+2P_{10}^4-5P_{10}^2)\frac{(P_{20}-1)\sin^3 L}{(\cos L+1)^3}+ \\
&+ (P_{20}^4-6P_{20}^3-P_{10}^2P_{20}^2+13P_{20}^2-6P_{10}^2P_{20}-12P_{20}-2P_{10}^4+7P_{10}^2+4)\frac{P_{10}\sin^2 L}{(\cos L+1)^2}+
\end{aligned}
$$

$$
\begin{aligned}
&+ \ (P_{20}^5 - 5P_{20}^4 - P_{10}^2P_{20}^3 + 3P_{20}^3 - 7P_{10}^2P_{20}^2 + 5P_{20}^2 - 2P_{10}^4P_{20} -\\
&+ \ 3P_{10}^2P_{20} - 4P_{20} - 2P_{10}^4 + 11P_{10}^2)\frac{\sin L}{(\cos L+1)} - P_{10}(P_{20}^4 - P_{10}^2P_{20}^2 - 3P_{20}^2 - P_{10}^2 + 4]/\\
&/ \ [(P_{20}-1)^4\frac{\sin^4 L}{(\cos L+1)^4} - 4P_{10}(P_{20}-1)^3\frac{\sin^3 L}{(\cos L+1)^3} -\\
&+ \ 2(P_{20}-1)^2(P_{20}^2 - 2P_{10}^2 - 1)\frac{\sin^2 L}{(\cos L+1)^2} +\\
&+ \ 4P_{10}(P_{20}-1)^2(P_{20}+1)\frac{\sin L}{(\cos L+1)} + (P_{20}-1)^2(P_{20}+1)^2])\Bigg)
\end{aligned}
$$

$$
\begin{aligned}
\Phi_{s3}(L) \ = \ &\frac{1}{\sigma^2}\left(\frac{3P_{10}}{\sqrt{\sigma}}\arctan\frac{\frac{(P_{20}-1)\sin L}{\cos L+1} - P_{10}}{\sqrt{\sigma}} +\right.\\
&+ \ [3P_{10}(P_{20}-1)\frac{\sin^3 L}{(\cos L+1)^3} +\\
&+ \ (2P_{20}^4 + 4P_{10}^2P_{20}^2 - 4P_{20}^2 - 9P_{10}^2P_{20} + 2P_{10}^4 + 5P_{10}^2 + 2)\frac{\sin^2 L}{(\cos L+1)^2} -\\
&+ \ P_{10}(5P_{20}^2 - 4P_{10}^2 - 5)\frac{\sin L}{(\cos L+1)} - (P_{20}+1)(2P_{20}^2 - P_{10}^2 - 2)]/\\
&/ \ [(P_{20}-1)^3\frac{\sin^4 L}{(\cos L+1)^4} - 4P_{10}(P_{20}-1)^2\frac{\sin^3 L}{(\cos L+1)^3} -\\
&+ \ 2(P_{20}-1)(P_{20}^2 - 2P_{10}^2 - 1)\frac{\sin^2 L}{(\cos L+1)^2} +\\
&+ \ \left.4P_{10}(P_{20}-1)^2\frac{\sin L}{(\cos L+1)} + (P_{20}-1)(P_{20}+1)^2]\right)
\end{aligned}
$$

$$
\begin{aligned}
\Phi_{c3}(L) \ = \ &\frac{1}{\sigma^2}\left(\frac{3P_{20}}{\sqrt{\sigma}}\arctan\frac{\frac{(P_{20}-1)\sin L}{\cos L+1} - P_{10}}{\sqrt{\sigma}} +\right.\\
&+ \ [(2P_{20}^4 + 3P_{20}^3 + 4P_{10}^2P_{20}^2 + 2P_{20}^2 - 3P_{20} + 2P_{10}^4 - 4P_{10}^2 + 2)\frac{(P_{20}-1)\sin^3 L}{(\cos L+1)^3} -\\
&+ \ (2P_{20}^4 - 9P_{20}^3 + 4P_{10}^2P_{20}^2 + 14P_{20}^2 - 9P_{20} + 2P_{10}^4 - 4P_{10}^2 + 2)\frac{P_{10}\sin^2 L}{(\cos L+1)^2} +\\
&+ \ (-2P_{20}^5 + 3P_{20}^4 + (-4P_{10}^2 - 1)P_{20}^3 + (-8P_{10}^2 - 1)P_{20}^2 + (-2P_{10}^4 + 8P_{10}^2 + 3)P_{20} -\\
&+ \ 2P_{10}^4 + 4P_{10}^2 - 2+)\frac{\sin L}{(\cos L+1)} - P_{10}P_{20}(5P_{20}^2 + 2P_{10}^2 - 5)]/\\
&/ \ [(P_{20}-1)^4\frac{\sin^4 L}{(\cos L+1)^4} - 4P_{10}(P_{20}-1)^3\frac{\sin^3 L}{(\cos L+1)^3} -\\
&+ \ 2(P_{20}-1)^2(P_{20}^2 - 2P_{10}^2 - 1)\frac{\sin^2 L}{(\cos L+1)^2} +
\end{aligned}
$$

$$+\ \ 4P_{10}(P_{20}-1)^2(P_{20}+1)\frac{\sin L}{(\cos L+1)}+(P_{20}-1)^2(P_{20}+1)^2])\Bigg)$$

$$\begin{aligned}
\Phi_{s5}(L) &= \frac{1}{4\sigma^4}\Bigg(\frac{5P_{10}(3P_{20}^2+3P_{10}^2+4)}{\sqrt{\sigma}}\arctan\frac{\frac{(P_{20}-1)\sin L}{\cos L+1}-P_{10}}{\sqrt{\sigma}}+\\
&+ [15P_{10}(P_{20}-1)^6(3P_{20}^2+3P_{10}^2+4)\frac{\sin^7 L}{(\cos L+1)^7}+\\
&+ 3(P_{20}-1)^2(8P_{20}^8+32P_{10}^2P_{20}^6-32P_{20}^6-105P_{10}^2P_{20}^5+48P_{10}^4P_{20}^4+219P_{10}^2P_{20}^4+48P_{20}^4-105P_{10}^4P_{20}^3-\\
&+ 455P_{10}^2P_{20}^3+32P_{10}^6P_{20}^2+219P_{10}^4P_{20}^2+621P_{10}^2P_{20}^2-32P_{20}^2-315P_{10}^4P_{20}-420P_{10}^2P_{20}+8P_{10}^8-32P_{10}^6+\\
&+ 153P_{10}^4+108P_{10}^2+8)\frac{\sin^6 L}{(\cos L+1)^6}-\\
&+ P_{10}(P_{20}-1)(32P_{20}^8+165P_{20}^7+128P_{10}^2P_{20}^6-623P_{20}^6-615P_{10}^2P_{20}^5+550P_{20}^5+192P_{10}^4P_{20}^4+1461P_{10}^2P_{20}^4-\\
&+ 138P_{20}^4-780P_{10}^4P_{20}^3-3050P_{10}^2P_{20}^3-55P_{20}^3+128P_{10}^6P_{20}^2+1956P_{10}^4P_{20}^2+4614P_{10}^2P_{20}^2+\\
&+ 477P_{20}^2-2340P_{10}^4P_{20}-3615P_{10}^2P_{20}-660P_{20}+32P_{10}^8-128P_{10}^6+972P_{10}^4+1077P_{10}^2+252)\frac{\sin^5 L}{(\cos L+1)^5}-\\
&+ (72P_{20}^9-16P_{10}^2P_{20}^8-72P_{20}^8-537P_{10}^2P_{20}^7-288P_{20}^7-64P_{10}^4P_{20}^6+2251P_{10}^2P_{20}^6+288P_{20}^6+\\
&+ 357P_{10}^4P_{20}^5-3614P_{10}^2P_{20}^5+432P_{20}^5-96P_{10}^6P_{20}^4-15P_{10}^4P_{20}^4+2418P_{10}^2P_{20}^4-432P_{20}^4+\\
&+ 1038P_{10}^6P_{20}^3+736P_{10}^4P_{20}^3+1139P_{10}^2P_{20}^3-288P_{20}^3-64P_{10}^8P_{20}^2-2346P_{10}^6P_{20}^2-4728P_{10}^4P_{20}^2-\\
&+ 3825P_{10}^2P_{20}^2+288P_{20}^2+72P_{10}^8P_{20}+1962P_{10}^6P_{20}+5907P_{10}^4P_{20}+3012P_{10}^2P_{20}+72P_{20}-\\
&+ 16P_{10}^10-8P_{10}^8-558P_{10}^6-2193P_{10}^4-828P_{10}^2-72)\frac{\sin^4 L}{(\cos L+1)^4}+\\
&+ P_{10}(32P_{20}^9+251P_{20}^8+128P_{10}^2P_{20}^7-566P_{20}^7-865P_{10}^2P_{20}^6-55P_{20}^6+192P_{10}^4P_{20}^5+1602P_{10}^2P_{20}^5+\\
&+ 484P_{20}^5-876P_{10}^4P_{20}^4-2219P_{10}^2P_{20}^4-319P_{20}^4+128P_{10}^6P_{20}^3+1752P_{10}^4P_{20}^3+2068P_{10}^2P_{20}^3+\\
&+ 602P_{20}^3+272P_{10}^6P_{20}^2-48P_{10}^4P_{20}^2+1377P_{10}^2P_{20}^2-201P_{20}^2+32P_{10}^8P_{20}-416P_{10}^6P_{20}-2616P_{10}^4P_{20}-\\
&+ 3798P_{10}^2P_{20}-552P_{20}+32P_{10}^8+16P_{10}^6+1596P_{10}^4+1707P_{10}^2+324)\frac{\sin^3 L}{(\cos L+1)^3}+\\
&+ (24P_{20}^10+96P_{10}^2P_{20}^8-24P_{20}^8-657P_{10}^2P_{20}^7+144P_{10}^4P_{20}^6+657P_{10}^2P_{20}^6-144P_{20}^6-321P_{10}^4P_{20}^5+\\
&+ 438P_{10}^2P_{20}^5+96P_{10}^6P_{20}^4+465P_{10}^4P_{20}^4-1014P_{10}^2P_{20}^4+336P_{20}^4+384P_{10}^6P_{20}^3+1426P_{10}^4P_{20}^3+\\
&+ 1095P_{10}^2P_{20}^3+24P_{10}^8P_{20}^2-192P_{10}^6P_{20}^2-2146P_{10}^4P_{20}^2-327P_{10}^2P_{20}^2-264P_{20}^2+48P_{10}^8P_{20}-\\
&+ 272P_{10}^6P_{20}-1105P_{10}^4P_{20}-876P_{10}^2P_{20}+24P_{10}^8-16P_{10}^6+1537P_{10}^4+588P_{10}^2+72)\frac{\sin^2 L}{(\cos L+1)^2}-\\
&+ P_{10}(147P_{20}^8-69P_{10}^2P_{20}^6-309P_{20}^6-264P_{10}^4P_{20}^4-489P_{10}^2P_{20}^4+45P_{20}^4-48P_{10}^6P_{20}^2+\\
&+ 224P_{10}^4P_{20}^2+1185P_{10}^2P_{20}^2+249P_{20}^2-16P_{10}^6+40P_{10}^4-627P_{10}^2-132)\frac{\sin L}{(\cos L+1)}-\\
&+ (P_{20}+1)(24P_{20}^8-3P_{10}^2P_{20}^6-48P_{20}^6-33P_{10}^4P_{20}^4-78P_{10}^2P_{20}^4-6P_{10}^6P_{20}^2+28P_{10}^4P_{20}^2+\\
&+ 165P_{10}^2P_{20}^2+48P_{20}^2-2P_{10}^6+5P_{10}^4-84P_{10}^2-24)]/\\
&/ [3(P_{20}-1)^7\frac{\sin^8 L}{(\cos L+1)^8}-24P_{10}(P_{20}-1)^6\frac{\sin^7 L}{(\cos L+1)^7}-\\
&+ 12(P_{20}-1)^5(P_{20}^2-6P_{10}^2-1)\frac{\sin^6 L}{(\cos L+1)^6}+24P_{10}(P_{20}-1)^4(3P_{20}^2-4P_{10}^2-3)\frac{\sin^5 L}{(\cos L+1)^5}+\\
&+ 6(P_{20}-1)^3(3P_{20}^4-24P_{10}^2P_{20}^2-6P_{20}^2+8P_{10}^4+24P_{10}^2+3)\frac{\sin^4 L}{(\cos L+1)^4}-\\
&+ 24P_{10}(P_{20}-1)^3(P_{20}+1)(3P_{20}^2-4P_{10}^2-3)\frac{\sin^3 L}{(\cos L+1)^3}-12(P_{20}-1)^3(P_{20}+1)^2(P_{20}^2-6P_{10}^2-1)\frac{\sin^2 L}{(\cos L+1)^2}+\\
&+ 24P_{10}(P_{20}-1)^3(P_{20}+1)^3\frac{\sin L}{(\cos L+1)}+3(P_{20}-1)^3(P_{20}+1)^4]\Bigg)
\end{aligned}$$

$$\begin{aligned}
\Phi_{c5}(L) &= \frac{1}{4\sigma^4}\Bigg(\frac{5P_{20}(3P_{20}^2+3P_{10}^2+4)}{\sqrt{\sigma}}\arctan\frac{\frac{(P_{20}-1)\sin L}{\cos L+1}-P_{10}}{\sqrt{\sigma}}+\\
&+ [3(P_{20}-1)^3(8P_{20}^8-15P_{20}^7+32P_{10}^2P_{20}^6+28P_{20}^6-15P_{10}^2P_{20}^5-110P_{20}^5+48P_{10}^4P_{20}^4-36P_{10}^2P_{20}^4+\\
&+ 188P_{20}^4-90P_{10}^2P_{20}^3-135P_{20}^3+32P_{10}^6P_{20}^2-96P_{10}^4P_{20}^2+156P_{10}^2P_{20}^2+
\end{aligned}$$

$$
\begin{aligned}
&+ \quad 48P_{20}^2 - 15P_{10}^2P_{20} - 20P_{20} + 8P_{10}^8 - 32P_{10}^6 + 48P_{10}^4 - 32P_{10}^2 + 8)\frac{\sin^7 L}{(\cos L+1)^7} - \\
&+ \quad 3P_{10}(P_{20}-1)^2(24P_{20}^8 - 105P_{20}^7 + 96P_{10}^2P_{20}^6 + 324P_{20}^6 - 105P_{10}^2P_{20}^5 - 770P_{20}^5 + 144P_{10}^4P_{20}^4 + \\
&+ \quad 132P_{10}^2P_{20}^4 + 1124P_{20}^4 - 630P_{10}^2P_{20}^3 - 945P_{20}^3 + 96P_{10}^6P_{20}^2 - 288P_{10}^4P_{20}^2 + 708P_{10}^2P_{20}^2 + \\
&+ \quad 464P_{20}^2 - 105P_{10}^2P_{20} - 140P_{20} + 24P_{10}^8 - 96P_{10}^6 + 144P_{10}^4 - 96P_{10}^2 + 24)\frac{\sin^6 L}{(\cos L+1)^6} - \\
&+ \quad (P_{20}-1)(40P_{20}^10 - 133P_{20}^9 + 64P_{10}^2P_{20}^8 + 428P_{20}^8 + 743P_{10}^2P_{20}^7 - 1173P_{20}^7 - 144P_{10}^4P_{20}^6 - \\
&+ \quad 2844P_{10}^2P_{20}^6 + 1408P_{20}^6 + 972P_{10}^4P_{20}^5 + 4511P_{10}^2P_{20}^5 - 83P_{20}^5 - 416P_{10}^6P_{20}^4 - 2880P_{10}^4P_{20}^4 - \\
&+ \quad 6512P_{10}^2P_{20}^4 - 1252P_{20}^4 + 128P_{10}^6P_{20}^3 + 4296P_{10}^4P_{20}^3 + 8229P_{10}^2P_{20}^3 + 1137P_{20}^3 - 344P_{10}^8P_{20}^2 + \\
&+ \quad 704P_{10}^6P_{20}^2 - 3168P_{10}^4P_{20}^2 - 5460P_{10}^2P_{20}^2 - 552P_{20}^2 + 32P_{10}^8P_{20} - 128P_{10}^6P_{20} + 972P_{10}^4P_{20} + \\
&+ \quad 1077P_{10}^2P_{20} + 252P_{20} - 96P_{10}^10 + 312P_{10}^8 - 288P_{10}^6 - 48P_{10}^4 + 192P_{10}^2 - 72)\frac{\sin^5 L}{(\cos L+1)^5} - \\
&+ \quad P_{10}(128P_{20}^10 - 809P_{20}^9 + 464P_{10}^2P_{20}^8 + 2644P_{20}^8 - 11P_{10}^2P_{20}^7 - 5289P_{20}^7 + 576P_{10}^4P_{20}^6 - \\
&+ \quad 1620P_{10}^2P_{20}^6 + 5744P_{20}^6 + 846P_{10}^4P_{20}^5 + 1183P_{10}^2P_{20}^5 - 1279P_{20}^5 + 224P_{10}^6P_{20}^4 - 4824P_{10}^4P_{20}^4 - \\
&+ \quad 4024P_{10}^2P_{20}^4 - 4676P_{20}^4 + 64P_{10}^6P_{20}^3 + 4308P_{10}^4P_{20}^3 + 11067P_{10}^2P_{20}^3 + 6261P_{20}^3 - 64P_{10}^8P_{20}^2 - \\
&+ \quad 512P_{10}^6P_{20}^2 - 1080P_{10}^4P_{20}^2 - 9348P_{10}^2P_{20}^2 - 3696P_{20}^2 + 16P_{10}^8P_{20} - 64P_{10}^6P_{20} + 846P_{10}^4P_{20} + \\
&+ \quad 1761P_{10}^2P_{20} + 1116P_{20} - 48P_{10}^10 + 48P_{10}^8 + 288P_{10}^6 - 672P_{10}^4 + 528P_{10}^2 - 144)\frac{\sin^4 L}{(\cos L+1)^4} + \\
&+ \quad (40P_{20}^11 - 147P_{20}^10 + 64P_{10}^2P_{20}^9 + 457P_{20}^9 + 1185P_{10}^2P_{20}^8 - 871P_{20}^8 - 144P_{10}^4P_{20}^7 - 3235P_{10}^2P_{20}^7 + \\
&+ \quad 181P_{20}^7 + 1116P_{10}^4P_{20}^6 + 3053P_{10}^2P_{20}^6 + 1523P_{20}^6 - 416P_{10}^6P_{20}^5 - 2772P_{10}^4P_{20}^5 - 3135P_{10}^2P_{20}^5 - \\
&+ \quad 1641P_{20}^5 - 432P_{10}^6P_{20}^4 + 1656P_{10}^4P_{20}^4 + 1843P_{10}^2P_{20}^4 + 83P_{20}^4 - 344P_{10}^8P_{20}^3 + 1264P_{10}^6P_{20}^3 + \\
&+ \quad 2712P_{10}^4P_{20}^3 + 4407P_{10}^2P_{20}^3 + 711P_{20}^3 - 312P_{10}^8P_{20}^2 + 144P_{10}^6P_{20}^2 - 4068P_{10}^4P_{20}^2 - \\
&+ \quad 6273P_{10}^2P_{20}^2 - 516P_{20}^2 - 96P_{10}^10P_{20} + 344P_{10}^8P_{20} - 272P_{10}^6P_{20} + 1548P_{10}^4P_{20} + 1899P_{10}^2P_{20} + \\
&+ \quad 252P_{20} - 96P_{10}^10 + 312P_{10}^8 - 288P_{10}^6 - 48P_{10}^4 + 192P_{10}^2 - 72)\frac{\sin^3 L}{(\cos L+1)^3} - \\
&+ \quad P_{10}(72P_{20}^10 - 513P_{20}^9 + 288P_{10}^2P_{20}^8 + 1098P_{20}^8 + 255P_{10}^2P_{20}^7 - 795P_{20}^7 + 432P_{10}^4P_{20}^6 + \\
&+ \quad 66P_{10}^2P_{20}^6 - 732P_{20}^6 + 1248P_{10}^4P_{20}^5 - 623P_{10}^2P_{20}^5 + 2397P_{20}^5 + 288P_{10}^6P_{20}^4 - 1200P_{10}^4P_{20}^4 - \\
&+ \quad 2852P_{10}^2P_{20}^4 - 2046P_{20}^4 + 624P_{10}^6P_{20}^3 - 1616P_{10}^4P_{20}^3 + 2049P_{10}^2P_{20}^3 - 357P_{20}^3 + 72P_{10}^8P_{20}^2 - \\
&+ \quad 96P_{10}^6P_{20}^2 + 112P_{10}^4P_{20}^2 + 2786P_{10}^2P_{20}^2 + 1536P_{20}^2 + 144P_{10}^8P_{20} - 528P_{10}^6P_{20} + 592P_{10}^4P_{20} - \\
&+ \quad 1681P_{10}^2P_{20} - 732P_{20} + 72P_{10}^8 - 288P_{10}^6 + 432P_{10}^4 - 288P_{10}^2 + 72)\frac{\sin^2 L}{(\cos L+1)^2} - \\
&+ \quad (24P_{20}^11 - 75P_{20}^10 + 96P_{10}^2P_{20}^9 + 123P_{20}^9 + 357P_{10}^2P_{20}^8 + 45P_{20}^8 + 144P_{10}^4P_{20}^7 - 69P_{10}^2P_{20}^7 - \\
&+ \quad 453P_{20}^7 + 696P_{10}^4P_{20}^6 - 279P_{10}^2P_{20}^6 + 291P_{20}^6 + 96P_{10}^6P_{20}^5 - 120P_{10}^4P_{20}^5 - 1065P_{10}^2P_{20}^5 + \\
&+ \quad 381P_{20}^5 + 336P_{10}^6P_{20}^4 - 944P_{10}^4P_{20}^4 - 609P_{10}^2P_{20}^4 - 393P_{20}^4 + 24P_{10}^8P_{20}^3 + 144P_{10}^6P_{20}^3 - \\
&+ \quad 496P_{10}^4P_{20}^3 + 1953P_{10}^2P_{20}^3 - 15P_{20}^3 + 72P_{10}^8P_{20}^2 - 176P_{10}^6P_{20}^2 + 104P_{10}^4P_{20}^2 + \\
&+ \quad 627P_{10}^2P_{20}^2 + 108P_{20}^2 + 72P_{10}^8P_{20} - 304P_{10}^6P_{20} + 472P_{10}^4P_{20} - 915P_{10}^2P_{20} - 60P_{20} + 24P_{10}^8 - \\
&+ \quad 96P_{10}^6 + 144P_{10}^4 - 96P_{10}^2 + 24)\frac{\sin L}{(\cos L+1)} - \\
&+ \quad P_{10}P_{20}(99P_{20}^8 + 177P_{10}^2P_{20}^6 - 117P_{20}^6 + 102P_{10}^4P_{20}^4 - 205P_{10}^2P_{20}^4 - 243P_{20}^4 + 24P_{10}^6P_{20}^2 - \\
&+ \quad 4P_{10}^4P_{20}^2 - 121P_{10}^2P_{20}^2 + 441P_{20}^2 + 24P_{10}^6 - 98P_{10}^4 + 149P_{10}^2 - 180)]/ \\
&/ \quad [3(P_{20}-1)^8\frac{\sin^8 L}{(\cos L+1)^8} - 24P_{10}(P_{20}-1)^7\frac{\sin^7 L}{(\cos L+1)^7} - \\
&+ \quad 12(P_{20}-1)^6(P_{20}^2 - 6P_{10}^2 - 1)\frac{\sin^6 L}{(\cos L+1)^6} + 24P_{10}(P_{20}-1)^5(3P_{20}^2 - 4P_{10}^2 - 3)\frac{\sin^5 L}{(\cos L+1)^5} + \\
&+ \quad 6(P_{20}-1)^4(3P_{20}^4 - 24P_{10}^2P_{20}^2 - 6P_{20}^2 + 8P_{10}^4 + 24P_{10}^2 + 3)\frac{\sin^4 L}{(\cos L+1)^4} - \\
&+ \quad 24P_{10}(P_{20}-1)^4(P_{20}+1)(3P_{20}^2 - 4P_{10}^2 - 3)\frac{\sin^3 L}{(\cos L+1)^3} - 12(P_{20}-1)^4(P_{20}+1)^2(P_{20}^2 - 6P_{10}^2 - 1)\frac{\sin^2 L}{(\cos L+1)^2} + \\
&+ \quad 24P_{10}(P_{20}-1)^4(P_{20}+1)^3\frac{\sin L}{(\cos L+1)} + 3(P_{20}-1)^4(P_{20}+1)^4]\Big)
\end{aligned}
$$